Stationary shear flows of nematic liquid crystals: A comprehensive study via Ericksen-Leslie model

Jia Jiao*, Kaiyin Huang†, and Weishi Liu‡

Abstract

We apply the Ericksen-Leslie dynamic model to investigate stationary solutions of planar shear flows for nematic liquid crystals. Nematic material is extremely rich and involves several parameters to characterize the basic local properties. The Ericksen-Leslie model of the nematic material includes Frank's parameters for Oseen-Frank energy and Leslie's dynamic parameters. Even in this simple setting of shear flows, the dynamics supported by the material exhibit quick rich behavior. With the aid of a Hamiltonian formulation and phase plane portraits, we are able to provide a rather complete picture about the possible solutions. In particular, we establish the existence of multiple solutions for the boundary value problem in many situations. We also try to explain the physical reasons for some of the results.

Keywords: Nematic liquid crystals, Ericksen-Leslie equations, Shear flow, Hamiltonian function, Phase plane portraits analysis.

1 Introduction

In this work, we will provide a detailed and comprehensive characterization for stationary planar shear flows of nematic liquid crystals. Even for this simplest setting, the behavior is extremely rich due mainly to the multi-parameter structure of the liquid crystal materials.

As is known, three common states of matter, solid, liquid and gas, are familiar to many people. Some substances may present multiple states when the temperature and pressure are varied. However, the classification of matters into three states is oversimplified. Liquid crystal material, for instance, is not one of the three states, which exhibits an intermediate phase between the solid crystal state and the isotropic liquid state. Thus, liquid crystals not only possess many of the mechanical properties of a liquid, e.g., high fluidity, inability to support shear, break-up and coalescence of droplets, but also are similar to crystals in that they exhibit anisotropy in their optical, electrical, and magnetic properties. Therefore, liquid crystal, as a kind of typical soft material, has been widely and successfully applied in life and industry, especially in display imaging technology. Despite liquid crystals' impressive technological applications, they are still poorly understood at a basic and fundamental level.

Generally, the discovery of liquid crystal is attributed to Austrian botanist F. Reinitzer ([33]) in 1888, and an English translation of his work ([34]) was published in the next year. In the same

*College of Science, Dalian Minzu University, Dalian, Liaoning 116600, P. R. China (jiaojia@dlnu.edu.cn).
†School of Mathematics, Sichuan University, Chengdu, Sichuan 610000, P. R. China (huangky1010@163.com).
‡Department of Mathematics, University of Kansas, Lawrence, Kansas 66045, USA (wsliu@ku.edu).

year, German physicist Lehmann ([21]) first used “flowing crystals” to describe these materials and he coined a new term “liquid crystal” later around 1900 which remains in use today. In 1907, Vorländer ([36]) discovered that an essential prerequisite for the occurrence of two melting points was a rod-like molecule. His discovery was of crucial importance for the theoretical development of liquid crystals because it allowed theoreticians to mathematically describe the molecular structure as rod-like. So far, the description of rod-like is still used commonly. In 1922, Friedel ([17]) described different liquid crystal phases and proposed three broad categories: nematic, cholesteric and smectic. And this classification has been widely adopted and remains in usage nowadays.

Although liquid crystals were first discovered in 1888, it was until the mid 1930s that the synthesis and important physical properties of liquid crystals have accumulated to a systematic extent. After twenty years of slow development, the correct theory of liquid crystals was established until the end of the 1950s. At the same time, due to the liquid crystal’s application value in the thermal image object, researchers were inspired to explore further usage of liquid crystals in technology. In the late 1960s, researchers believed that liquid crystals will have a bright foreground in display device respect because of the discovery of dynamic scattering. Currently, the wide range of applications of liquid crystals has created new areas of academic and industrial research. Nowadays there are many reviews, textbooks and monographs on the theory, applications and rheology of liquid crystals are available (see, e.g., [9, 15, 19, 24, 35]).

A number of attempts have been made to formulate continuum theories to describe properties of liquid crystals. One of the most well-known continuum theories for flows of liquid crystals is the Ericksen-Leslie theory. The earliest attempt of static theory dates back to Oseen ([29]), from 1925 onwards, and Zocher ([37]) in 1927. Later on, Frank ([16]) established the static theory of liquid crystals in 1958. The attempt of dynamic theory for nematic liquid crystals was made by Anzelius ([1]) in 1931. However, the first widely accepted dynamic theory was formulated by Ericksen ([14]) in 1961 who proceeded to generalize the static theory of nematics in order to propose balance laws for their dynamical behaviour. Making use of these ideas, Leslie ([22, 23, 24]) managed successfully to formulate the constitutive equations and therefore complete the dynamic theory for nematic liquid crystals. These work led to the celebrated Ericksen-Leslie dynamic theory of nematic liquid crystals.

It should be mentioned that with the aid of the key verification of this theory provided by the experimental observations of Fisher and Frederickson ([18]), the Ericksen-Leslie dynamic theory was established as the generally accepted dynamic theory for nematic liquid crystals. Until now, the Ericksen-Leslie dynamic theory ([13, 23, 25]) has been successful in describing various flow phenomena in nematic liquid crystals. The stability of planar shear flows and nonplanar flow instabilities for nonaligning liquid crystals have been the subject of many experimental and theoretical investigations during the recent decades ([2, 5, 11, 24, 30]).

In this work, we will consider stationary behavior of planar shear flows of nematics via the Ericksen-Leslie model. This is probably the simplest setting of non-equilibrium problem of nematics. Nevertheless, due to the multi-parameter structure of the nematic material, even in this simplest setting, the dynamics supported by the material exhibit quick rich behavior. It is our hope that, with a good and systematic understanding, one can take the advantage of the rich structure and design simple (magnetic and/or electric) external forcing to create desired performance (like in the spring-mass system with forcing targeting at ‘degenerate’ behavior). This is one of the reasons for a great deal of treatments conducted previously. However, the problem was not completely understood. The present study relies on an important ingredient –

a Hamiltonian formulation of the system. With the help of this structure, we are able to provide the following.

(i) *A complete characterization of possible solutions and various representations:* The Hamiltonian structure of the (reduced) system for the director allows one to effectively sketch the phase plane portraits for all cases in terms of different range of Frank's and Lieslie's parameters. As a result, one can visualize all possibilities of solutions for the boundary value problem (BVP). For a better understanding about the solutions initially represented from the phase plane portrait, we also provide other representations, including the graph of the angle function of the director.

(ii) *Detailed analytical results:* Another important role of the Hamiltonian structure is the explicit Hamiltonian function which, together with the visualization of the orbits, allows us to conduct the analytical study of the solutions; in particular, conditions for various types of solutions are given in concrete manners (although implicitly in terms of integrations of relevant physical quantities of the nematics in general). Multiple solutions are shown to exist depending on various ranges of Frank's and Lieslie's parameters. As a consequence, hysteresis occurs in this simple setting of shear flows of nematics.

(iii) *Physical interpretations of analytical results:* Because the concrete conditions in terms of Frank's and Lieslie's parameters for the results established, we are able to extract qualitative and quantitive information and interpret the theoretical funding from physical point of views. This would provide insights for choice of specific nematic material for purposes of designs using solution structures of the problem.

The rest is organized as follows. In Section 2, a short background of nematics and the Ericksen-Leslie model for the shear flow are recalled and the BVP to be examined in the work is specified. In Section 3, we start with a Hamiltonian formulation of the shear flow, present sketches of phase plane portraits for all possible parameter ranges, and classify all possible types of solutions. In Sections 4, 5 and 6, detailed analyses are conducted toward more quantitative understanding of all types of solutions. We also try to interpret the results in terms of Frank's and Leslie's parameters as well as relevant system quantities. Section 7 contains a conclusion remark and a discussion for further research topics related to this work.

2 Background and models for shear flows of nematics

2.1 The Ericksen-Leslie dynamic models for nematics

A basic theory that describes the dynamics of nematic liquid crystals is the Ericksen-Leslie dynamic theory, proposed by Leslie ([22, 23]) in the sixties. This theory generalized Ericksen's static theory of nematic liquid crystals ([14]) by proposing balance laws for their dynamical behavior. It accounts for fluid anisotropy and elastic stresses resulting from spatial distortion of the director field, and has consistently been applied in many flow problems of nematic liquid crystals. Due to the complexity of Ericksen-Leslie dynamic equations, numerical methods have been widely used (e.g. [3, 4, 10, 20, 28]) to investigate the behavior of solutions of these equations, while few consider them by analytical approaches (see, e.g., [7, 26, 27]).

A nematic material is characterized by its velocity field $v = (v_1, v_2, v_3)$ and director field $n = (n_1, n_2, n_3)$. In the following, we will use Einstein's summation convention and denote, for any smooth function f of the spatial variable $x = (x_1, x_2, x_3)$, the partial derivative $\partial_{x_j} f$ by $f_{,j}$. The usual material time derivative is denoted by a superposed dot. The Ericksen-Leslie dynamic equations for the velocity field $v(t, x)$ and the director field $n(t, x)$ of nematics in the incompressible isothermal case when the director inertial term is neglected can be stated concisely as follows (see [23], for example). They consist of the constraints

$$n_i n_i = 1 \text{ and } v_{i,i} = 0, \tag{2.1}$$

together with the balance laws which arise from linear and angular momentum, namely,

$$\begin{aligned} \rho \dot{v}_i &= \rho F_i - (p + w_F)_{,i} + \tilde{g}_j n_{j,i} + G_j n_{j,i} + \tilde{t}_{ij,j}, \\ (\frac{\partial w_F}{\partial n_{i,j}})_{,j} &- \frac{\partial w_F}{\partial n_i} + \tilde{g}_i + G_i = \lambda n_i, \end{aligned} \tag{2.2}$$

where ρ is the density, F_i is the external body force per unit mass, p is the pressure, w_F is the Oseen-Frank elastic energy density given in (2.8) below, and G_i is the generalized body force. The scalar function λ is a Lagrange multiplier which can usually be eliminated or evaluated by taking the scalar product of equation (2.2) with n; it arises from the constraint that n is a unit vector. Constitutive relations for the viscous stress $\widetilde{t}_{ij}$ and the vector $\widetilde{g}_i$ are

$$\begin{aligned} \tilde{t}_{ij} =& \alpha_1 n_k A_{kp} n_p n_i n_j + \alpha_2 N_i n_j + \alpha_3 n_i N_j + \alpha_4 A_{ij} \\ &+ \alpha_5 n_j A_{ik} n_k + \alpha_6 n_i A_{jk} n_k, \\ \tilde{g}_i =& - \gamma_1 N_i - \gamma_2 A_{ip} n_p, \end{aligned} \tag{2.3}$$

where

$$A_{ij} = \frac{1}{2}(v_{i,j} + v_{j,i}), \quad N_i = \dot{n}_i - W_{ij} n_j, \quad W_{ij} = \frac{1}{2}(v_{i,j} - v_{j,i}), \tag{2.4}$$

and α_1, α_2, …, α_6 are the Leslie viscosity parameters, A_{ij} is the rate of strain tensor, W_{ij} is the vorticity tensor, N_i is the co-rotational time flux of the director $\mathbf{n}$ and a superposed dot again represents the material time derivative. The coefficient γ_1 is often referred to as the twist or rotational viscosity and γ_2 is called the torsion coefficient. The Parodi relation

$$\gamma_2 = \alpha_3 + \alpha_2 = \alpha_6 - \alpha_5 \tag{2.5}$$

is assumed to hold and the Leslie viscosities must additionally satisfy the inequalities

$$\begin{aligned} &\alpha_4 > 0, \quad \gamma_1 = \alpha_3 - \alpha_2 > 0, \quad 2\alpha_4 + \alpha_5 + \alpha_6 > 0, \\ &2\alpha_1 + 3\alpha_4 + 2\alpha_5 + 2\alpha_6 > 0, \quad 4\gamma_1(2\alpha_4 + \alpha_5 + \alpha_6) > (\alpha_2 + \alpha_3 + \gamma_2)^2. \end{aligned} \tag{2.6}$$

The stress tensor for nematic liquid crystals is given by

$$t_{ij} = -p\delta_{ij} - \frac{\partial w_F}{\partial n_{p,j}} + \tilde{t}_{ij}, \tag{2.7}$$

where the elastic energy for nematics is

$$\begin{aligned} w_F =& \frac{1}{2}(K_1 - K_2 - K_4)(n_{i,i})^2 + \frac{1}{2} K_2 n_{i,j} n_{i,j} + \frac{1}{2} K_4 n_{i,j} n_{j,i} \\ &+ \frac{1}{2}(K_3 - K_2) n_j n_{i,j} n_k n_{i,k}, \end{aligned} \tag{2.8}$$

where K_i's are Frank's parameters.

2.2 Shear flow of nematics and stationary boundary value problem

In this work, we investigate in detail a simple shear flow of nematic liquid crystals discussed by Leslie ([23]). Without loss of generality, consider a fluid layer of prescribed thickness between parallel plates at a distance d apart which are parallel to the xz-plane. Assume that the upper plate at $y = d$ while the lower plate at $y = 0$, and the two plates slide past each other at a prescribed slip velocity in the x direction. The state of the nematic liquid crystal is described by its velocity $\mathbf{v} = \mathbf{v}(x, y, z, t)$ and its director $\mathbf{n} = \mathbf{n}(x, y, z, t)$ with $|\mathbf{n}| = 1$. Since liquid crystals generally lack polarity, the vectors $\mathbf{n}$ and $-\mathbf{n}$ are indistinguishable.

Here we consider the simple planar shear flow of the form

$$\mathbf{n} = \big(\cos\phi\,(y,t)\,, \sin\phi\,(y,t)\,, 0\big), \quad \mathbf{v} = \big(v(y,t), 0, 0\big), \tag{2.9}$$

where ϕ is the angle of the director from the x-axis. Clearly, the above satisfy the constraints (2.1). Suppose also that there are no external body force F and generalized body force G. The governing Ericksen-Leslie dynamic equations become ([7, 23, 25], etc.), for $y \in (0, d)$,

$$\begin{aligned}
&\rho\frac{\partial v}{\partial t} = \frac{\partial}{\partial y}\left(g(\phi)\frac{\partial v}{\partial y} + h(\phi)\frac{\partial \phi}{\partial t}\right),\\
&\gamma_1\frac{\partial \phi}{\partial t} = f(\phi)\frac{\partial^2 \phi}{\partial y^2} + \frac{1}{2}\frac{\partial f(\phi)}{\partial \phi}\left(\frac{\partial \phi}{\partial y}\right)^2 - h(\phi)\frac{\partial v}{\partial y},
\end{aligned} \tag{2.10}$$

where f, g and h are periodic functions with period π and are given by

$$\begin{aligned}
f(\phi) =& K_1\cos^2\phi + K_3\sin^2\phi,\\
g(\phi) =& \alpha_1\sin^2\phi\cos^2\phi + \frac{\alpha_5-\alpha_2}{2}\sin^2\phi + \frac{\alpha_6+\alpha_3}{2}\cos^2\phi + \frac{\alpha_4}{2},\\
h(\phi) =& \alpha_3\cos^2\phi - \alpha_2\sin^2\phi = \frac{\gamma_1+\gamma_2\cos(2\phi)}{2}.
\end{aligned} \tag{2.11}$$

The last identity in the definition of h follows from the relations in (2.5) and (2.6). It is clear that $f(\phi) > 0$ for all ϕ (i.e., $K_1, K_3 > 0$) and it is known that $g(\phi) > 0$ under (2.5) and (2.6).

For stationary shear flow, Ericksen-Leslie system (2.10) is, for $0 < y < d$,

$$\frac{\mathrm{d}}{\mathrm{d}y}\left(g(\phi)\frac{\mathrm{d}v}{\mathrm{d}y}\right) = 0, \quad f(\phi)\frac{\mathrm{d}^2\phi}{\mathrm{d}y^2} + \frac{1}{2}\frac{\mathrm{d}f}{\mathrm{d}\phi}\left(\frac{\mathrm{d}\phi}{\mathrm{d}y}\right)^2 - h(\phi)\frac{\mathrm{d}v}{\mathrm{d}y} = 0. \tag{2.12}$$

We will study this system together with the boundary conditions

$$v(0) = v_0,\ v(d) = v_d; \quad \phi(0) = \phi_0,\ \phi(d) = \phi_d. \tag{2.13}$$

Remark 2.1. Recall that, for the director at one location, its angle ϕ is only defined up to an integer multiple of π. In the following, we will look for smooth solutions of BVP (2.12) and (2.13) with fixed $\phi(0) = \phi_0$ but $\phi(d) = \phi_d + m\pi$ for any integer m.

Integrate the first equation in (2.12) to get

$$\frac{\mathrm{d}v}{\mathrm{d}y} = \frac{a}{g(\phi)}, \tag{2.14}$$

with a being a constant

$$a = \frac{v_d - v_0}{\int_0^d g^{-1}(\phi) \mathrm{d}y}. \tag{2.15}$$

Note that a is unknown and is to be determined as a part of the problem.

Remark 2.2. If $v_d = v_0$, then $a = 0$, and hence, $v(y) = v_d = v_0$. Equation (2.16) can be reduced to $f(\phi)\phi'^2 = C$ for some constant C. So $\phi(y)$ is monotone and the boundary value problem can be analyzed easily. In the following, we will consider $v_0 \neq v_d$. For definiteness, we will assume $v_0 < v_d$ so that $a > 0$.

BVP (2.12) and (2.13) is reduced to, for some a (to be determined later on by (2.15)),

$$f(\phi)\frac{\mathrm{d}^2\phi}{\mathrm{d}y^2} + \frac{1}{2}f'(\phi)\left(\frac{\mathrm{d}\phi}{\mathrm{d}y}\right)^2 = \frac{ah(\phi)}{g(\phi)} \tag{2.16}$$

and, for some integer $m \geq 0$ (see Remark 2.3),

$$\phi(0) = \phi_0, \quad \phi(d) = \phi_d + m\pi. \tag{2.17}$$

Remark 2.3. Note that, if $\phi(y)$ is a solution of (2.16) with $\phi(0) = \phi_0$ and $\phi(d) = \phi_d + m\pi$, then $\phi^*(y) = \phi(d-y) - m\pi$ is a solution with $\phi^*(0) = \phi_d$ and $\phi^*(d) = \phi_0 - m\pi$. So we may assume $m \geq 0$ in (2.17). For simplicity, we also assume ϕ_0, $\phi_d \in [0, \pi)$ and $\phi_0 \leq \phi_d$ in (2.17).

The dynamics and stability of planar shear flow and nonplanar flow instabilities for nonaligning liquid crystals have been the subject of many experimental and theoretical investigations. It is well known that, when Leslie viscosities $\alpha_2 < 0$ and $\alpha_3 < 0$, nematic liquid crystals align uniformly in shear flow. Particularly, only for the case of $\alpha_2 \leq \alpha_3 \leq 0$, Currie and MacSithigh ([11]) considered some simplified cases for planar shear flow by the phased-plane approach. When $\alpha_2 < 0 < \alpha_3$, the uniformly aligned configurations become unstable for sufficiently high shear rates and either tumbling regimes develop in the flow region in the shear plane or the alignment of nematic liquid crystals takes on a component perpendicular to the shear plane. In this case, Pan ([30, 31, 32]) used Ericksen-Leslie model to investigate the solution branch of simple planar shear flow between moving parallel plates for non-flow-orienting nematic liquid crystals. He showed the existence of solutions of planar shear flow and analyzed the tumbling phenomenon along the solution branches. In [12], Dorn and Liu studied shear flows of a fluid layer between two solid blocks via a liquid-crystal type model proposed in [8]. They provided a characterization of the existence and multiplicity of steady-states. Furthermore, their stability result suggests that this simple model exhibits hysteresis, which is also supported by numerical simulations. The model studied in [12], by Dorn and Liu is oversimplified comparing to the present model. It turns out multiple solutions exist for Ericken-Leslie model in many situations as shown later in this paper.

3 BVP (2.16) and (2.17) for $a > 0$

We will treat a in (2.15) as a *given* constant first and analyze BVP (2.16) and (2.17). In this way, any solution $\phi(y; a)$ depends on the constant a. The full problem will then be analyzed by treating (2.15) as a fixed point problem for a.

3.1 A Hamiltonian structure for equation (2.16)

It is known that equation (2.16) has a first integral (see, e.g., display (6.18) in [23]), which helps one get quantity information about solutions to a certain extent. It turns out a Hamiltonian formulation of system (2.16) is much more appropriate for a systematic analysis of the problem as a dynamical system. We thus will take this formulation. To do so, we denote derivatives with respect to y by primes, and introduce

$$\eta = f(\phi)\phi'. \tag{3.1}$$

Equation (2.16) is then converted to the system

$$\phi' = \frac{\eta}{f(\phi)}, \quad \eta' = \frac{f_\phi(\phi)}{2f^2(\phi)}\eta^2 + \frac{ah(\phi)}{g(\phi)}. \tag{3.2}$$

The following result can be verified directly.

Proposition 3.1. *System (3.2) is a Hamiltonian system*

$$\phi' = \frac{\partial H}{\partial \eta}(\phi,\eta) \ \ \text{and} \ \ \eta' = -\frac{\partial H}{\partial \phi}(\phi,\eta)$$

with the Hamiltonian function

$$H(\phi,\eta) = \frac{\eta^2}{2f(\phi)} - \frac{a}{2}G(\phi), \tag{3.3}$$

where

$$G(\phi) = \int_{\phi_0}^{\phi} \frac{2h(t)}{g(t)}\mathrm{d}t. \tag{3.4}$$

Remark 3.1. Not surprisingly, the Hamiltonian function $H(\phi,\eta)$ in (3.3) is equivalent to the first integral in display (6.18) of reference [23].

System (3.2) will be viewed as a dynamical system with phase space $\mathbb{R}^2$. With the help of the Hamiltonian structure, the phase plane portraits of (3.2) can be readily sketched, which helps one visualize all types of solutions of BVP (2.16) and (2.17). There are several major cases that are distinguished in terms of the liquid crystal material parameters/quantities. Each case has its own dynamical behavior, some can be explicitly quantified and some are implicitly.

3.2 Major cases and corresponding phase plane portraits

We begin with a rough classification of the phase plane portraits of system (3.2) based on whether or not it has equilibria. Note that $(\phi,0)$ is an equilibrium of system (3.2) if and only if $h(\phi)=0$, or equivalently, $\gamma_1+\gamma_2\cos(2\phi)=0$.

The phase plane portrait is clearly symmetric with respect to the ϕ-axis. In the upper half plane $\{\eta>0\}$, the orbit with level $H(\phi,\eta)=C$ is given by the graph of the function

$$\eta = \eta(\phi;C) = \sqrt{(aG(\phi)+2C)f(\phi)}. \tag{3.5}$$

Case I. $\gamma_1 > |\gamma_2|$: In this case, system (3.2) has no equilibrium. Since $G'(\phi)>0$, the function $\eta=\eta(\phi;C)=\sqrt{(aG(\phi)+2C)f(\phi)}$ in (3.5) is defined for $\phi \ge \phi_C$ with $aG(\phi_C)=-2C$ and

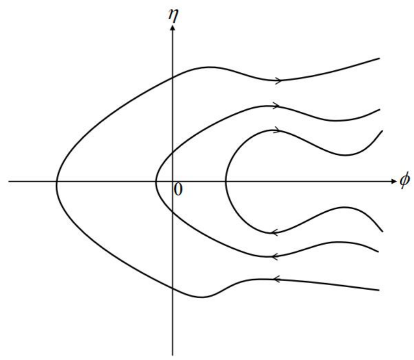

Figure 1: *Sketch of the phase plane portrait for Case I:* $\gamma_1 > |\gamma_2|$.

approaches ∞ as $\phi \to \infty$. Figure 1 is a sketch of the phase plane portrait in this case. We note that, in $\{\eta > 0\}$, the graph of the function $\eta = \eta(\phi; C)$ is not monotonic in general.

Case II. $|\gamma_2| = \gamma_1 > 0$**:** In this case, one has

$$h(\phi) = \gamma_1 \sin^2 \phi \ \text{ if } \ \gamma_2 < 0 \ \text{ and } \ h(\phi) = \gamma_1 \cos^2 \phi \ \text{ if } \ \gamma_2 > 0.$$

Thus, if $\gamma_2 < 0$, then $(n\pi, 0)$'s are equilibria; if $\gamma_2 > 0$, then $((n + 1/2)\pi, 0)$'s are equilibria. In either case, $G'(\phi) \geq 0$, and one obtains the following result easily.

Proposition 3.2. *If* $|\gamma_2| = \gamma_1 > 0$, *then each equilibrium is a cusp with its stable and unstable manifolds to its right-hand side (see Figure 2).*

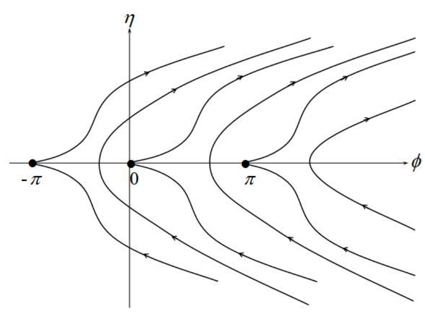

Figure 2: *Sketch of the phase plane portrait for Case II with* $-\gamma_2 = \gamma_1$.

Case III. $|\gamma_2| \geq \gamma_1 > 0$**:** Concerning equilibria, one has

Proposition 3.3. *For* $|\gamma_2| \geq \gamma_1 > 0$, *system (3.2) has equilibria* $(\phi^* + n\pi, 0)$ *and* $(\phi^{**} + n\pi, 0)$ *for all integers* n *with* $\phi^* = \frac{1}{2} \arccos(-\gamma_1/\gamma_2) \in (0, \pi/2)$ *and* $\phi^{**} = \pi - \phi^* \in (\pi/2, \pi)$. *Furthermore,*

(i) if $\gamma_2 > \gamma_1 > 0$, *then* $(\phi^* + n\pi, 0)$ *are saddles and* $(\phi^{**} + n\pi, 0)$ *are centers;*

(ii) if $-\gamma_2 > \gamma_1 > 0$, *then* $(\phi^{**} + n\pi, 0)$ *are saddles and* $(\phi^* + n\pi, 0)$ *are centers.*

Proof. The eigenvalues of the linearization at the equilibria $(\phi^* + n\pi, 0)$ are

$$\lambda^*_\pm = \pm \sqrt{\frac{a\gamma_2 \sin(2\phi^*)}{f(\phi^*) g(\phi^*)}},$$

and those at $(\phi^{**}+n\pi,0)$ are

$$\lambda_{\pm}^{**} = \pm\sqrt{\frac{a\gamma_2\sin(2\phi^{**})}{f(\phi^*)g(\phi^*)}} = \pm\sqrt{-\frac{a\gamma_2\sin(2\phi^{*})}{f(\phi^*)g(\phi^*)}}.$$

Note that $\sin(2\phi^*)>0$. Therefore, if $\gamma_2>0$, then $(\phi^*+n\pi,0)$ are saddles and $(\phi^{**}+n\pi,0)$ are centers; if $\gamma_2<0$, then $(\phi^*+n\pi,0)$ are centers and $(\phi^{**}+n\pi,0)$ are saddles. □

Subcase III1. $\int_0^\pi \frac{h(t)}{g(t)}\mathrm{dt}=0$**:** In this case, for $\gamma_2<0$, $(\phi^{**}+n\pi,0)$'s are saddles and connected by heteroclinic cycles that enclose periodic orbits around the center $(\phi^*+n\pi,0)$, as sketched in the left panel of Figure 3. For $\gamma_2>0$, $(\phi^*+n\pi,0)$'s are saddles with $H(\phi^*+n\pi,0)=H(\phi^*,0)$ for all integers n, and hence, for each integer n, adjacent saddles $(\phi^*+n\pi,0)$ and $(\phi^*+(n+1)\pi,0)$ are connected by a heteroclinic cycle that encloses periodic orbits around the center $(\phi^{**}+n\pi,0)$, as shown in the right panel of Figure 3.

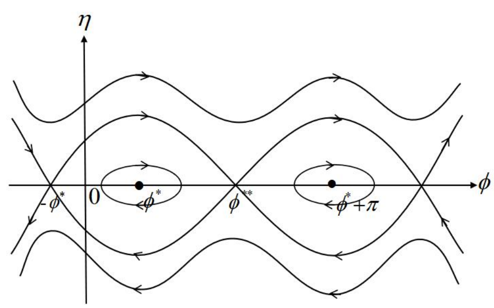

Figure 3: *Phase plane portrait for Case III1 where* $\int_0^\pi \frac{h(t)}{g(t)}\mathrm{dt}=0$*. Left panel:* $-\gamma_2>\gamma_1>0$*; Right panel:* $\gamma_2>\gamma_1>0$*.*

Subcase III2. $\int_0^\pi \frac{h(t)}{g(t)}\mathrm{dt}\neq 0$**:** For $\int_0^\pi \frac{h(t)}{g(t)}\mathrm{dt}<0$, one has $G(\phi)\to-\infty$ as $\phi\to\infty$ and $G(\phi)\to\infty$ as $\phi\to-\infty$, and hence, the function $\eta=\eta(\phi;C)=\sqrt{(aG(\phi)+2C)f(\phi)}$ in (3.5) is defined for $\phi\le\phi_C$ with $aG(\phi_C)=-2C$. For $\gamma_2<0$, $(\phi^{**}+n\pi,0)$ is a saddle with a homoclinic orbit to the right-hand side that encloses periodic orbits around the center $(\phi^*+(n+1)\pi)$, as sketched in the left panel of Figure 4.

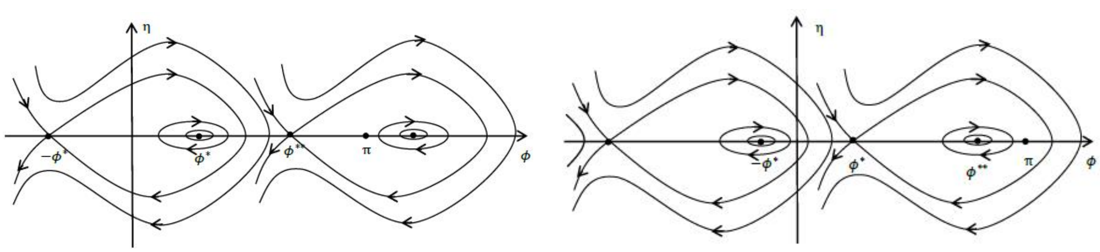

Figure 4: *Phase plane portrait for Case III2 with* $\int_0^\pi \frac{h(t)}{g(t)}\mathrm{dt}<0$*. Left panel:* $-\gamma_2>\gamma_1>0$*; Right panel:* $\gamma_2>\gamma_1>0$*.*

Similarly, for $\int_0^\pi \frac{h(t)}{g(t)}\mathrm{dt}<0$, for each saddle, the associated homoclinic orbit is on its left hand side, as sketched in Figure 5.

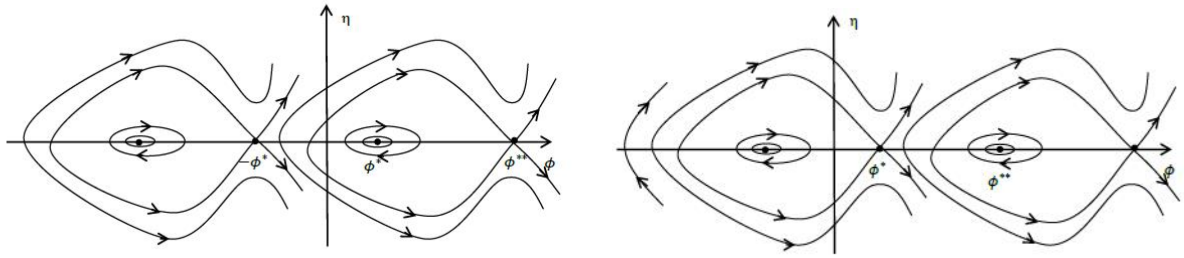

Figure 5: *Phase plane portrait for Case III2 with* $\int_0^\pi \frac{h(t)}{g(t)}\mathrm{dt} > 0$. *Left panel:* $-\gamma_2 > \gamma_1 > 0$. *Right panel:* $\gamma_2 > \gamma_1 > 0$.

3.3 Classification and representations of solutions

Recall that we are interested in solutions (ϕ, η) of system (3.2) with boundary conditions $\phi(0) = \phi_0$ and $\phi(d) = \phi_d + m\pi$ with $0 \le \phi_0 \le \phi_d < \pi$ and some integer $m \ge 0$.

We will classify each solution (ϕ, η) based on the number of (interior) extrema of $\phi(y)$ in $(0, d)$ and the types of first and last extrema; more precisely, we say *the solution is an* (σ_1, σ_2)*-p-vibrating solution* where $\sigma_1 = l$ (or r) if the first extremum is a minimum (or maximum), $\sigma_2 = l$ (or r) if the last extremum is a minimum (or maximum), and $p \ge 0$ is the number of total extrema. Since minimum and maximum alternate, $\sigma_1 = \sigma_2$ if p is odd and $\sigma_1 \ne \sigma_2$ if p is even. If $p = 0$, there is no need to use (σ_1, σ_2) and we will call it a *monotone* solution; if $p = 1$, then we will replace (σ_1, σ_2)-p-vibrating with σ-p-vibrating with $\sigma = l$ or r for the type of the only extremum.

Associated to each solution $\phi = \phi(y)$, one also has the map $\mathbf{n} : [0, d] \to \mathbb{S}^1 \to \mathbb{P}^1$ given by $\phi(y)$ as its (polar) angle followed by projection $\mathbb{S}^1 \to \mathbb{P}^1$ since ϕ and $\phi + \pi$ are identified for the director $\mathbf{n}$. To its (oriented) image we add the shorter arc between the angle ϕ_0 and ϕ_d with the orientation moving from $\phi_d \to \phi_0$. In this way, we can define *the winding number* of the solution by that of the extended oriented closed curve. In particular, any solution $\phi = \phi(y)$ with $\phi(d) = \phi_d + m\pi$ has winding number m and we call it *an* m*-winding solution.* The winding number is also the *degree* of the corresponding map $\mathbf{n} : [0, d] \to \mathbb{P}^1$.

For 0-vibrating and m-winding solutions, we often call them *monotone* m-winding solutions; for 1-vibrating and m-winding solutions, we often call them *non-monotone* m-winding solutions.

We now provide different representations of possible solutions. The existence and uniqueness/multiplicity will be analyzed in the next sections.

Representation by orbits in the phase plane portraits. Due to the Hamiltonian structure, the simplest representation of the solutions is associated with the phase plane portrait. Each solution is represented by the orbit $\{(\phi(y), \eta(y)) : \ y \in [0, d]\}$ in the phase plane. While m-winding solutions may occur in both Case I ($\gamma_1 > |\gamma_2|$), Case II ($\gamma_1 = |\gamma_2|$), and Case III ($|\gamma_2| > \gamma_1 > 0$), p-vibrating solutions may only occur in Case III and the corresponding orbit will remain inside of one heteroclinic loop or one homoclinic orbit.

In Figure 6 for Case I, *only winding solutions exist.* Arcs labelled **a** and **b** are monotone m-winding solutions and arc **c** represents a non-monotone m-winding solution. Similarly, *only winding solutions exist for Case II* as illustrated in Figure 7. But there are major differences between the solution structures for Case I and Case II as shown in later sections.

In Figure 8, illustrated are types of solutions in Case III1 with $\int_0^\pi \frac{h(t)}{g(t)}\mathrm{dt} = 0$ where adjacent saddles are connected by heteroclinic loops. In particular, various *vibrating solutions* within the

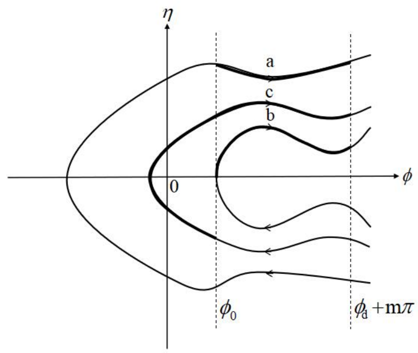

Figure 6: *Three types of solutions in Case I for $m \geq 0$: arcs* **a** *and* **b** *represent two monotone solutions and arc* **c** *represents a non-monotone solution.*

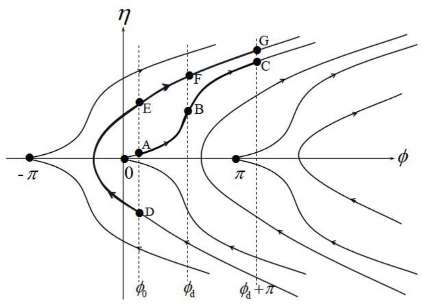

Figure 7: *Three types of solutions in Case II with $\gamma_2 < 0$ for $m \geq 0$: arcs AB, EF are two monotone* 0*-winding solutions and DEF is non-monotone* 0*-winding solution; arcs ABC, EFG are two monotone* 1*-winding solutions and DEFG is a non-monotone* 1*-winding solution.*

first heteroclinic loops are presented.

For Case III2 with $\gamma_2 > \gamma_1 > 0$ and $\int_0^\pi \frac{h(t)}{g(t)}\mathrm{dt} < 0$, in addition to possible vibrating solutions within the first homoclinic orbit similar to those in Figure 8, monotone and non-monotone m-winding solutions are represented in Figure 9.

Representation by the graph of $\phi(y)$. One can also represent the solution using the graph of $\phi(y)$. See Figure 10.

4 Case I: $\gamma_1 > |\gamma_2|$: No equilibria

Recall that $\gamma_1 = \alpha_3 - \alpha_2$ and $\gamma_2 = \alpha_3 + \alpha_2$. One checks easily that $\gamma_1 > |\gamma_2|$ when either (i) $\gamma_2 = \alpha_3 + \alpha_2 > 0 > \alpha_2$ or (ii) $\gamma_2 = \alpha_3 + \alpha_2 < 0 < \alpha_3$.

There is no equilibria in this case and the only possible solutions are m-winding solutions. We will present our results with two considerations:

(i) *for system (2.16) or (3.2) with fixed a and $(v_d - v_0)$ from (2.15) (as a design parameter);*

(ii) *for system (2.16) or (3.2) with a from the nonlocal constraint (2.15) with fixed $(v_d - v_0)$.*

For Case II and Case III, for simplicity, we will only present the study for the first consideration, that is, for fixed $a > 0$.

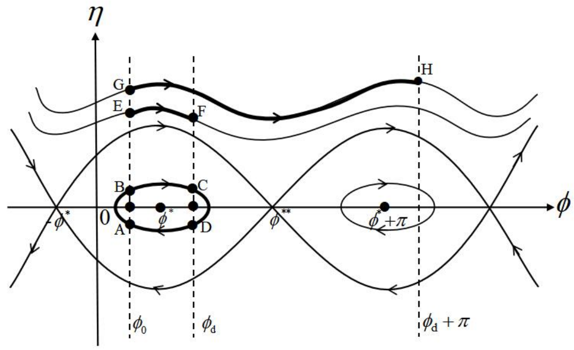

Figure 8: *Types of solutions in Case III1 with* $-\gamma_2 > \gamma_1 > 0$ *and* $\int_0^\pi \frac{h(t)}{g(t)}\mathrm{dt} = 0$*: monotone* 0*-winding solutions represented by the arc EF from E to F and the arc BC, monotone* 1*-winding solution represented by the arc GH; the arc ABC represents a non-monotone (* l*-*1*-vibrating) solution, the arc BCD represents a non-monotone (*r*-*1*-vibrating) solution, the arc ABCD represents a* (l,r)*-*2*-vibrating solution, etc.*

4.1 BVP (2.16) and (2.17) with fixed $a > 0$

It follows from Proposition 3.1 that if $(\phi(y), \eta(y))$ is a solution with $(\phi(0), \eta(0)) = (\phi_0, \eta_0)$, then

$$\frac{\eta^2}{2f(\phi)} - \frac{a}{2}G(\phi) = H(\phi_0, \eta_0) = \frac{\eta_0^2}{2f(\phi_0)}. \tag{4.1}$$

Recall that $\eta = f(\phi)\phi'$. Equation (4.1) becomes

$$\phi'^2 = \frac{a(G(\phi) + c)}{f(\phi)} \quad \text{where} \quad c = \frac{\eta_0^2}{af(\phi_0)} \geq 0. \tag{4.2}$$

4.1.1 Monotone m-winding solutions for fixed $m \geq 0$

For monotone m-winding solutions with $m \geq 0$, $\phi'(y) > 0$ is positive, and hence,

$$\frac{\mathrm{d}\phi}{\mathrm{d}y} = \sqrt{\frac{aG(\phi) + 2c}{f(\phi)}} \quad \text{or} \quad \frac{\sqrt{f(\phi)}}{\sqrt{a(G(\phi)+c)}}\mathrm{d}\phi = \mathrm{d}y. \tag{4.3}$$

Integrating from $y = 0$ to $y = d$, one gets

$$M_m(c) = \sqrt{a}d \quad \text{where} \quad M_m(c) = \int_{\phi_0}^{\phi_d + m\pi} \frac{\sqrt{f(\phi)}}{\sqrt{G(\phi) + c}}\mathrm{d}\phi. \tag{4.4}$$

Lemma 4.1. *For fixed* $m \geq 0$*,* $M_m(c)$ *is decreasing in* $c \geq 0$*, and*

$$\lim_{c\to+\infty} M_m(c) = 0 \quad \textit{and} \quad M_m(0) < \infty.$$

Proof. The first two statements are clear. Note that, for $\phi \geq \phi_0$,

$$G(\phi) = G(\phi_0) + G'(\tilde{\phi})(\phi - \phi_0) = G'(\tilde{\phi})(\phi - \phi_0) = \frac{2h(\tilde{\phi})}{g(\tilde{\phi})}(\phi - \phi_0)$$

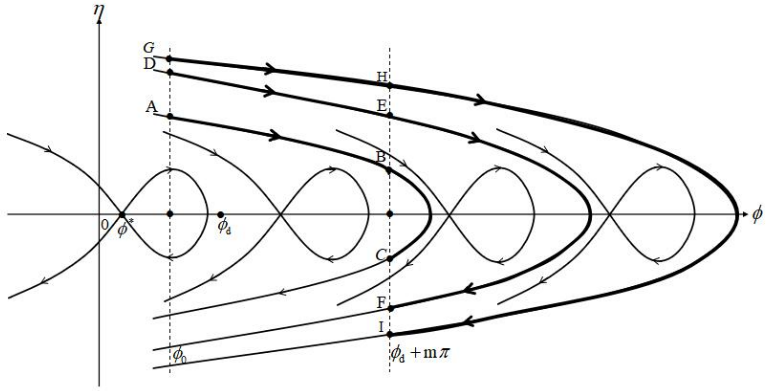

Figure 9: *For Case III2 with $\gamma_2 > \gamma_1 > 0$ and $\int_0^\pi \frac{h(t)}{g(t)}\mathrm{dt} < 0$ (homoclinic orbits to the right-hand side of saddles $(\phi^* + n\pi, 0)$: in addition to possible solutions within the first homoclinic orbits as those in Case III1 above, the arcs AB, DE, GH represent three monotone m-winding solutions; the arcs ABC, DEF, GHI represent three non-monotone m-winding solutions.*

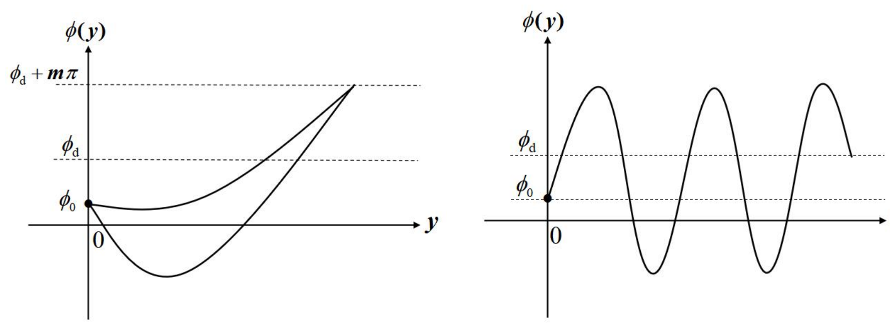

Figure 10: *The graphs of $\phi(y)$. Left: top graph corresponds to a monotone m-winding solution and the bottom one is a non-monotone m-winding solution; Right: a (r,r)-5-vibrating solution.*

for some $\tilde{\phi}$, and hence, $|G(\phi)| < C_1(\phi - \phi_0)$ for some $C_1 > 0$. Thus, for some constant $C_2 > 0$,

$$M_m(0) = \int_{\phi_0}^{\phi_d+m\pi} \frac{\sqrt{f(\phi)}}{\sqrt{G(\phi)}}\mathrm{d}\phi < C_2 \int_{\phi_0}^{\phi_d+m\pi} (\phi - \phi_0)^{-1/2}\mathrm{d}\phi = 2C_2(\phi_d + m\pi - \phi_0)^{1/2}.$$

This completes the proof. $\square$

Let $a_m > 0$ be defined as

$$\sqrt{a_m} = \frac{1}{d}\int_{\phi_0}^{\phi_d+m\pi} \frac{\sqrt{f(\phi)}}{\sqrt{G(\phi)}}\mathrm{d}\phi = \frac{M_m(0)}{d}. \tag{4.5}$$

One sees from the proof of $M_{m,a}(0) < \infty$ that a_m is well-defined.

The main result for this case is as follows.

Theorem 4.2. *Assume $\gamma_1 > |\gamma_2|$. For any given $m \geq 0$, one has*

(i) if $a > a_m$, then BVP (2.16) and (2.17) has no monotone m-winding solution;

(ii) if $a \leq a_m$, then BVP (2.16) and (2.17) has a unique monotone m-winding solution.

Proof. It follows from (4.5) that, if $a > a_m$, then $M_m(0) < \sqrt{a}d$. Lemma 4.1 then implies that, for $c \geq 0$, $M_m(c) \leq M_m(0) < \sqrt{a}d$, which yields the statement (i). If $a \leq a_m$, then $M_m(0) \geq \sqrt{a}d$. Lemma 4.1 insures that there is a unique $c = c(a) \in [0, \infty)$ such that $M_m(c) = \sqrt{a}d$, which implies (ii). See arcs **a** and **b** in Figure 6. □

Remark 4.1. For fixed $m \geq 0$ and $a > 0$, one can define

$$d_{m,a} = \frac{1}{\sqrt{a}} \int_{\phi_0}^{\phi_d + m\pi} \frac{\sqrt{f(\phi)}}{\sqrt{G(\phi)}} \mathrm{d}\phi = \frac{M_m(0)}{\sqrt{a}},$$

so that $M_m(c) = \sqrt{a}d$ has a unique solution $c \geq 0$ for $d \leq d_{m,a}$. As one decreases d, the orbit associated to the monotone solution moves up.

It is clear that a_m is increasing in m and $a_m \to \infty$ as $m \to \infty$. Thus, if $a > 0$ is fixed, then there is a unique $m_a \geq 0$ so that $a \leq a_m$ if and only if $m \geq m_a$, and hence, the BVP has a unique solution if and only if $m \geq m_a$. □

4.1.2 Non-monotone m-winding solutions for fixed $m \geq 0$

In this case, the only non-monotone solution would be l-0-vibrating solution. So we will simply call them *non-monotone* m-winding solutions.

For $\alpha < \phi_0$, let

$$N_m(\alpha) = 2N_1(\alpha) + N_2(\alpha; m) = 2\int_\alpha^{\phi_0} \frac{\sqrt{f(\phi)}}{\sqrt{G(\phi) - G(\alpha)}} \mathrm{d}\phi + \int_{\phi_0}^{\phi_d + m\pi} \frac{\sqrt{f(\phi)}}{\sqrt{G(\phi) - G(\alpha)}} \mathrm{d}\phi. \quad (4.6)$$

Note that $N_1(\alpha)$ does not depend on m. One can establish the next result easily.

Lemma 4.3. *The function $N_m(\alpha)$ is well-defined,*

$$\lim_{\alpha \to \phi_0^-} N_m(\alpha) = M_m(0) \quad \textit{and} \quad \lim_{\alpha \to -\infty} N_m(\alpha) = +\infty.$$

Proof. Since $G'(\phi)$ is bounded and non-zero, $l(\phi - \alpha) \leq G(\phi) - G(\alpha) \leq L(\phi - \alpha)$ for some $0 < l < L$, and hence, the improper integrals of $N_m(\alpha)$ converge. The first limit is easier to verify. For the other, it suffices to show that $\lim_{\alpha \to -\infty} N_1(\alpha) = +\infty$ since $0 < N_2(\alpha; m) \leq M_m(0)$. From the definition of G, one has

$$G(\phi) - G(\alpha) = \int_\alpha^\phi \frac{2h(t)}{g(t)} \,\mathrm{d}t < \int_\alpha^\phi \frac{\gamma_1 + |\gamma_2|}{g_*} \,\mathrm{d}t = \frac{\gamma_1 + |\gamma_2|}{g_*}(\phi - \alpha), \quad (4.7)$$

where $g_* := \min g(\phi)$. Therefore

$$\begin{aligned} N_1(\alpha) &= \int_\alpha^{\phi_0} \frac{\sqrt{f(\phi)}}{\sqrt{G(\phi) - G(\alpha)}} \,\mathrm{d}\phi > \int_\alpha^{\phi_0} \frac{\sqrt{K_1 \wedge K_3}}{\sqrt{\frac{\gamma_1 + |\gamma_2|}{g_*}(\phi - \alpha)}} \,\mathrm{d}\phi \\ &= \bar{C}_0 \int_\alpha^{\phi_0} \frac{1}{\sqrt{\phi - \alpha}} \,\mathrm{d}\phi = \bar{C}\sqrt{\phi_0 - \alpha}, \end{aligned}$$

which implies $\lim_{\alpha \to -\infty} N_1(\alpha) = +\infty$. □

The next result is easy to get.

Proposition 4.4. *The set of non-monotone m-winding solutions of BVP (2.16) and (2.17) is in one-to-one correspondence with the set of solutions $\alpha < \phi_0$ of equation $N_m(\alpha) = \sqrt{a}d$.*

The next result is on non-monotone m-winding solutions (see arc **c** in Figure 6).

Theorem 4.5. *If $a > a_m$, then BVP (2.16) and (2.17) has at least one non-monotone m-winding solution.*

Proof. If $a > a_m$, then $N_m(\alpha) < \sqrt{a}d$ for α close to ϕ_0. Lemma 4.6 then implies the result. $\square$

Combing Theorems 4.2 and 4.5, one has that, *for any $m \geq 0$ and $a > 0$, BVP (2.16) and (2.17) always has at least one m-winding solution.* We do not know whether or not it is possible that monotone and non-monotone solutions can co-exist for $a \leq a_m$.

While BVP (2.16) and (2.17) has a *unique monotone* m-winding solution for $a \leq a_m$ (Theorem 4.5), the remaining of this part is to show, under the condition that $a > a_m$, BVP (2.16) and (2.17) may have *multiple* non-monotone m-winding solutions (see Theorem 4.7 below).

Lemma 4.6. *Let $p : [0, 1] \to \mathbb{R}^+$ be a continuous and positive function. Consider*

$$S(\alpha) = \int_\alpha^{\frac{\pi}{2}} \frac{p(\cos^2\phi)\sin 2\phi}{\sqrt{G(\phi) - G(\alpha)}} \mathrm{d}\phi.$$

Then there exist $M_A, M_B \in \mathbb{R}^+$ and $m \in \mathbb{N}$ such that $S(-\frac{m\pi}{2}) = M_A > 0$, when m is an even number; and $S(-\frac{m\pi}{2}) = -M_B < 0$, when m is an odd number.

Proof. Note that

$$\begin{aligned} S(-\frac{m}{2}\pi) &= \int_{-\frac{m}{2}\pi}^{\frac{\pi}{2}} \frac{p(\cos^2\phi)\sin 2\phi}{\sqrt{G(\phi) - G(-\frac{m}{2}\pi)}} \, \mathrm{d}\phi = \sum_{k=0}^{m} \int_{-\frac{k}{2}\pi}^{-\frac{k-1}{2}\pi} \frac{p(\cos^2\phi)\sin 2\phi}{\sqrt{G(\phi) - G(-\frac{m}{2}\pi)}} \, \mathrm{d}\phi \\ &= \sum_{k=0}^{m} (-1)^k \int_{-\frac{k}{2}\pi}^{-\frac{k-1}{2}\pi} \frac{p(\cos^2\phi)|\sin 2\phi|}{\sqrt{G(\phi) - G(-\frac{m}{2}\pi)}} \, \mathrm{d}\phi. \end{aligned}$$

Set $a_k^m(\phi) = \int_{-\frac{k}{2}\pi}^{-\frac{k-1}{2}\pi} \frac{p(\cos^2\phi)|\sin 2\phi|}{\sqrt{G(\phi) - G(-\frac{m}{2}\pi)}} \, \mathrm{d}\phi$, and make the change of variables $\phi = -k\pi - \theta$ in $a_{k+1}^m(\phi)$. One then has

$$\begin{aligned} a_{k+1}^m(\phi) - a_k^m(\phi) &= \int_{-\frac{k+1}{2}\pi}^{-\frac{k}{2}\pi} \frac{p(\cos^2\phi)|\sin 2\phi|}{\sqrt{G(\phi) - G(-\frac{m}{2}\pi)}} \, \mathrm{d}\phi - \int_{-\frac{k}{2}\pi}^{-\frac{k-1}{2}\pi} \frac{p(\cos^2\phi)|\sin 2\phi|}{\sqrt{G(\phi) - G(-\frac{m}{2}\pi)}} \, \mathrm{d}\phi \\ &= \int_{-\frac{k}{2}\pi}^{-\frac{k-1}{2}\pi} \frac{p(\cos^2\phi)|\sin 2\phi|}{\sqrt{G(-k\pi - \phi) - G(-\frac{m}{2}\pi)}} \, \mathrm{d}\phi - \int_{-\frac{k}{2}\pi}^{-\frac{k-1}{2}\pi} \frac{p(\cos^2\phi)|\sin 2\phi|}{\sqrt{G(\phi) - G(-\frac{m}{2}\pi)}} \, \mathrm{d}\phi \\ &= \int_{-\frac{k}{2}\pi}^{-\frac{k-1}{2}\pi} p(\cos^2\phi)|\sin 2\phi| \left(\frac{1}{\sqrt{G(-k\pi - \phi) - G(-\frac{m}{2}\pi)}} - \frac{1}{\sqrt{G(\phi) - G(-\frac{m}{2}\pi)}} \right) \mathrm{d}\phi \\ &> \int_{-\frac{k}{2}\pi + \frac{\pi}{4}}^{-\frac{k-1}{2}\pi} p(\cos^2\phi)|\sin 2\phi| \left(\frac{1}{\sqrt{G(-k\pi - \phi) - G(-\frac{m}{2}\pi)}} - \frac{1}{\sqrt{G(\phi) - G(-\frac{m}{2}\pi)}} \right) \mathrm{d}\phi. \end{aligned}$$

Note that

$$\begin{aligned}
&\frac{1}{\sqrt{G(-k\pi-\phi)-G(-\frac{m}{2}\pi)}}-\frac{1}{\sqrt{G(\phi)-G(-\frac{m}{2}\pi)}}\\
&=\frac{G(\phi)-G(-k\pi-\phi)}{\sqrt{G(-k\pi-\phi)-G(-\frac{m}{2}\pi)}\sqrt{G(\phi)-G(-\frac{m}{2}\pi)}}\\
&\cdot\frac{1}{(\sqrt{G(-k\pi-\phi)-G(-\frac{m}{2}\pi)}+\sqrt{G(\phi)-G(-\frac{m}{2}\pi)})}.
\end{aligned}$$

Since for $\phi\in(-k\pi/2,-(k-1)\pi/2)$, one has

$$\begin{aligned}
G(\phi)-G(-k\pi-\phi)&=2\int_{-k\pi-\phi}^{\phi}\frac{h(t)}{g(t)}\,\mathrm{d}t>2\int_{-\frac{k}{2}\pi-\frac{\pi}{4}}^{-\frac{k}{2}\pi+\frac{\pi}{4}}\frac{h(t)}{g(t)}\,\mathrm{d}t\\
&=\begin{cases}4\int_0^{\frac{\pi}{4}}\frac{h(t)}{g(t)}\,\mathrm{d}t=\delta_1 & \textit{if } k \textit{ is even},\\ 4\int_{\frac{\pi}{4}}^{\frac{\pi}{2}}\frac{h(t)}{g(t)}\,\mathrm{d}t=\delta_2 & \textit{if } k \textit{ is odd}.\end{cases}
\end{aligned}$$

Thus

$$G(\phi)-G(-k\pi-\phi)>\delta_1\wedge\delta_2,$$

where $\delta_1\wedge\delta_2=\min\{\delta_1,\delta_2\}$;

$$\begin{aligned}
G(-k\pi-\phi)-G(-\frac{m}{2}\pi)&=\int_{-\frac{m}{2}\pi}^{-k\pi-\phi}\frac{h(t)}{g(t)}\,\mathrm{d}t<\int_{-\frac{m}{2}\pi}^{-\frac{k}{2}\pi}\frac{h(t)}{g(t)}\,\mathrm{d}t\\
&=(m-k)\int_0^{\frac{\pi}{2}}\frac{h(t)}{g(t)}\,\mathrm{d}t=(m-k)(\delta_1+\delta_2)
\end{aligned}$$

and

$$\begin{aligned}
G(\phi)-G(-\frac{m}{2}\pi)&=\int_{-\frac{m}{2}\pi}^{\phi}\frac{h(t)}{g(t)}\,\mathrm{d}t<\int_{-\frac{m}{2}\pi}^{-\frac{k-1}{2}\pi}\frac{h(t)}{g(t)}\,\mathrm{d}t\\
&=(m-k+1)\int_0^{\frac{\pi}{2}}\frac{h(t)}{g(t)}\,\mathrm{d}t=(m-k+1)(\delta_1+\delta_2),
\end{aligned}$$

we have

$$\begin{aligned}
a_{k+1}^m(\phi)-a_k^m(\phi)>&\frac{\delta_1\wedge\delta_2}{\sqrt{m-k}\sqrt{m-k+1}(\sqrt{m-k}+\sqrt{m-k+1})}\\
&\cdot\int_{-\frac{k}{2}\pi+\frac{\pi}{4}}^{-\frac{k-1}{2}\pi}p(\cos^2\phi)|\sin2\phi|\,\mathrm{d}\phi>\frac{c_*}{(m-k+1)^{\frac{3}{2}}},
\end{aligned}$$

where

$$c_*=\min\left\{(\delta_1\wedge\delta_2)\int_{-\frac{k}{2}\pi+\frac{\pi}{4}}^{-\frac{k-1}{2}\pi}p(\cos^2\phi)|\sin2\phi|\,\mathrm{d}\phi:k\in\mathbb{Z}\right\}$$

is independent of m. Therefore, for an even $m = 2n$, we have

$$S(-\frac{m}{2}\pi) = S(-n\pi) = \left(a_{2m}^{(2n)} - a_{2m-1}^{(2n)}\right) + \cdots + \left(a_2^{(2n)} - a_1^{(2n)}\right) + a_0^{(2n)}$$
$$> \frac{c_*}{1^{\frac{3}{2}}} + \frac{c_*}{2^{\frac{3}{2}}} + \cdots + \frac{c_*}{n^{\frac{3}{2}}} = c_* \sum_{k=1}^{n} \frac{1}{k^{\frac{3}{2}}} > c_* = M_A > 0,$$

where M_A is a lower bound being independent of n. For an odd $m = 2n+1$, we have

$$S(-\frac{m}{2}\pi) = -\left(a_{2n+1}^{(2n+1)} - a_{2n}^{(2n+1)}\right) - \cdots - \left(a_1^{(2n+1)} - a_0^{(2n+1)}\right)$$
$$< -\frac{c_*}{2^{\frac{3}{2}}} - \frac{c_*}{3^{\frac{3}{2}}} - \cdots - \frac{c_*}{(n+2)^{\frac{3}{2}}} = -c_* \sum_{k=2}^{n+2} \frac{1}{k^{\frac{3}{2}}} \leq \frac{-c_*}{2^{\frac{3}{2}}} = -M_B < 0.$$

where $-M_B$ is an upper bound which is independent of n. $\square$

Let

$$l(x) = l_0 + l_1 x^2 + l_2 x^4 + l_3 x^6, \tag{4.8}$$

where

$$\begin{aligned}
l_0 &= \alpha_1(-\alpha_2 + \alpha_4 + \alpha_5)K_1 \\
&\quad + [\alpha_1(2\alpha_2 + 2\alpha_3) + \alpha_2(\alpha_2 + 2\alpha_3 + \alpha_4 + \alpha_5) + \alpha_3(2\alpha_3 + 2\alpha_5)]K_3, \\
l_1 &= [\alpha_1(3\alpha_2 + 2\alpha_3) + \alpha_2(2 + \alpha_4 + \alpha_6) + \alpha_3(2 + \alpha_4 + \alpha_5)]K_1 \\
&\quad + [\alpha_1(-8\alpha_2 - 6\alpha_3) + \alpha_2(-4\alpha_2 - 8\alpha_3 - \alpha_4 - 2\alpha_5 + 2\alpha_6) \\
&\quad + \alpha_3(-4\alpha_3 - \alpha_4 - 3\alpha_5 + \alpha_5)]K_3, \\
l_2 &= [\alpha_1(-8\alpha_2 - 6\alpha_3) + \alpha_2(-3\alpha_2 - 6\alpha_3 - \alpha_5 + \alpha_6) + \alpha_3(-3\alpha_3 - \alpha_5 + \alpha_6)]K_1 \\
&\quad + [\alpha_1(12\alpha_2 + 10\alpha_3) + \alpha_2(3\alpha_2 + 6\alpha_3 + \alpha_5 - \alpha_6) + \alpha_3(3\alpha_3 + \alpha_5 - \alpha_6)]K_3, \\
l_3 &= 6\alpha_1(\alpha_2 + \alpha_3)K_1 - 6\alpha_1(\alpha_2 + \alpha_3)K_3.
\end{aligned}$$

A result on the existence of multiple solutions of BVP (2.16) and (2.17) is given as follows.

Theorem 4.7. *Assume $\gamma_1 > |\gamma_2|$ and $l(x) \geq 0$ for all $|x| \leq 1$ where $l(x)$ is defined in (4.8). Then there are infinite many α's such that $N_m'(\alpha) = 0$. In particular, if α_* is a local maximum of $N_m(\alpha)$ and $\sqrt{a_*}d = N_m(\alpha_*)$, then for a close to but smaller than a_*, $N_m(\alpha) = \sqrt{a}d$ has at least three solutions α's.*

Proof. From the definition of $N_m(\alpha)$ in (4.6), one has

$$N_m'(\alpha) = 2N_1'(\alpha) + N_2'(\alpha; m),$$

here $N_1(\alpha)$ can be divided into two terms,

$$N_1(\alpha) = N_{11}(\alpha) + N_{12}(\alpha) = \int_\alpha^{\frac{\pi}{2}} \frac{\sqrt{f(\phi)}}{\sqrt{G(\phi) - G(\alpha)}} \mathrm{d}\phi + \int_{\frac{\pi}{2}}^{\phi_0} \frac{\sqrt{f(\phi)}}{\sqrt{G(\phi) - G(\alpha)}} \mathrm{d}\phi.$$

The derivative of the first term of $N_1(\alpha)$ is

$$N_{11}'(\alpha) = \frac{-D(\alpha)\sqrt{f(\frac{\pi}{2})}}{D(\frac{\pi}{2})\sqrt{G(\frac{\pi}{2}) - G(\alpha)}} + \frac{D(\alpha)}{2} \int_\alpha^{\frac{\pi}{2}} \frac{A(\phi)\sin(2\phi)}{\sqrt{G(\phi) - G(\alpha)}} \mathrm{d}\phi, \tag{4.9}$$

where

$$A(\phi) = \frac{f'(\phi)D(\phi) - 2f(\phi)D'(\phi)}{D^2(\phi)\sqrt{f(\phi)}} = \frac{l(\cos^2\phi)}{D^2(\phi)g^2(\phi)\sqrt{f(\phi)}},$$
$$D(\phi) = \frac{\gamma_1 + \gamma_2\cos(2\phi)}{g(\phi)}, D'(\phi) = \frac{-2\gamma_2\sin(2\phi)g(\phi) - \gamma_2\cos(2\phi)g'(\phi)}{g^2(\phi)},$$
$$f = K_3 + (K_1 - K_3)\cos^2\phi, \quad f' = (K_3 - K_1)\sin(2\phi),$$
$$g(\phi) = \frac{1}{2}[2\alpha_1\sin^2\phi\cos^2\phi + (\alpha_5 - \alpha_2)\sin^2\phi + (\alpha_3 + \alpha_6)\cos^2\phi + \alpha_4]$$
$$= \frac{1}{2}(\alpha_4 + \alpha_5 - \alpha_2) + \frac{1}{2}(2\alpha_1 + \alpha_2 + \alpha_3 + \alpha_6 - \alpha_5)\cos^2\phi - \alpha_1\cos^4\phi,$$
$$g'(\phi) = \sin(2\phi)(\alpha_1\cos 2\phi - \gamma_2) = \sin(2\phi)[(-\alpha_1 - \gamma_2) + 2\alpha_1\cos^2\phi].$$

Then

$$\begin{aligned} l(\cos^2\phi) &= (K_3 - K_1)(\gamma_1 + \gamma_2\cos(2\phi))g(\phi) \\ &\quad + 2[K_3 + (K_1 - K_3)\cos^2\phi][2\gamma_2 g(\phi) + \gamma_2\cos(2\phi)(\alpha_1\cos(2\phi) - \gamma_2)] \\ &= l_0 + l_1\cos^2\phi + l_2\cos^4\phi + l_3\cos^6\phi. \end{aligned}$$

Applying Lemma 4.6 to the second term of N'_{11} in (4.9) with $p(\cos^2\phi) = A(\phi)$, we get

$$N'_{11}(-\frac{m\pi}{2}) = \begin{cases} < M_A < 0, m \text{ is a sufficiently large even number,} \\ > -M_B > 0, m \text{ is a sufficiently large odd number,} \end{cases} \tag{4.10}$$

and also easily get $\lim_{\alpha\to-\infty} N'_{12}(\alpha) = \lim_{\alpha\to-\infty} N'_2(\alpha; m) = 0$. Therefore, $N'_m(\alpha)$ changes sign infinitely many times as $\alpha \to -\infty$. So by the classical Zero Theorem, there are infinitely many α's (that are unbounded), such that $N'_m(\alpha) = 0$.

For the last statement, note that, near α_*, the graph of $N_m(\alpha)$ is a downward parabola-like curve. So there will be one α on each side of α_* with the same N-value, which is not the minimum of the function N_m. The statement follows since $N_m(\alpha) \to \infty$ as $\alpha \to -\infty$. □

Remark 4.2. We remark that the assumption $l(x) \geq 0$ for $|x| \leq 1$ in the theorem is possible. For example, if $\alpha_1 > 0$, $\alpha_4 \gg 1$, $\alpha_2 + \alpha_3 > 0$, and $K_1 \gg K_3$, then $l_0 \gg 1$, $l_1 \gg 1$ and $l_4 > 0$; in particular, one can make $\Delta = l_2^2 - 4l_1l_3 < 0$ so that $l_1 + l_2x^2 + l_3x^4 > 0$ for any x, and hence, $l(x) > 0$ for any x. □

Figure 11 contains the graphs of the functions of $N_m(\alpha)$ and $N'_m(\alpha)$ obtained by numerical computation for some special case. We see that there are infinitely stationary points of the function $N_m(\alpha)$, i.e. there are infinitely many points such that $N'_m(\alpha) = 0$.

4.2 Fixed $v_d - v_0$: The full BVP (2.12) and (2.13)

For solutions of BVP (2.12) and (2.13), we will call a solution $(v(y), \phi(y))$ of (2.12) *an m-winding solution* if its ϕ-component $\phi(y)$ is an m-winding solution of the corresponding planar system (2.16). We use other terminology in the similar way.

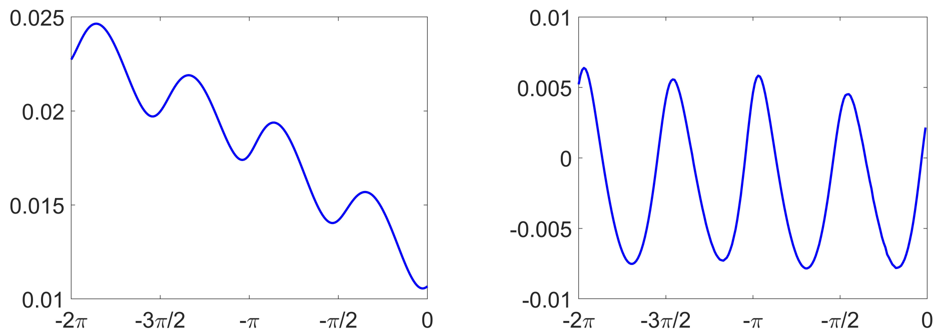

Figure 11: *The graphs of $N_m(\alpha)$ and $N_m'(\alpha)$: left for $N_m(\alpha)$ and right for $N_m'(\alpha)$.*

4.2.1 Monotone m-winding solutions for given $m \geq 0$

By (2.15) and (4.3), we obtain

$$v_d - v_0 = \int_0^d \frac{a}{g(\phi(y))}\,\mathrm{d}y = \int_{\phi_0}^{\phi_d+m\pi} \frac{\sqrt{a}}{g(\phi)} \cdot \frac{\sqrt{f(\phi)}}{\sqrt{G(\phi)+c}}\,\mathrm{d}\phi. \tag{4.11}$$

From (4.4) and (4.11), one obtains

$$\begin{aligned} H_m(c) := &\int_{\phi_0}^{\phi_d+m\pi} \frac{\sqrt{f(\phi)}}{\sqrt{G(\phi)+c}}\,\mathrm{d}\phi \int_{\phi_0}^{\phi_d+m\pi} \frac{\sqrt{f(\phi)}}{g(\phi)\sqrt{G(\phi)+c}}\,\mathrm{d}\phi \\ &= (v_d - v_0)d. \end{aligned} \tag{4.12}$$

One has

Proposition 4.8. *The set of monotone m-winding solutions of BVP (2.12) and (2.13) is in one-to-one correspondence with the set of solutions $c \geq 0$ of $H_m(c) = (v_d - v_0)d$.*

Proof. It is clear that a monotone m-winding solution $(v(y), \phi(y))$ of BVP (2.12) and (2.13) leads to a solution c of $H_m(c) = (v_d - v_0)d$. Assume now c is a solution of $H_m(c) = (v_d - v_0)d$. One can determine a from $M_m(c) = \sqrt{a}d$ in (4.4) and automatically $a \leq a_m$ since $M_m(c) < M_m(0) = \sqrt{a_m}d$. Theorem 4.1 then guarantees a unique monotone m-winding solution $\phi(y)$ of BVP (2.16) and (2.17) with the value a. □

We now work on the equation $H_m(c) = (v_d - v_0)d$.

Lemma 4.9. *(i) The function $H_m(c)$ is decreasing, $\lim_{c\to+\infty} H_m(c) = 0$, and $H_m(0)$ is finite.*

(ii) The function $H_m(0)$ is increasing in m and $\lim_{m\to+\infty} H_m(0) = \infty$.

Proof. (i) The first two statements follows from the definition of $H_m(c)$ in (4.12). Note that,

$$H_m(0) = \int_{\phi_0}^{\phi_d+m\pi} \frac{\sqrt{f(\phi)}}{\sqrt{G(\phi)}}\,\mathrm{d}\phi \int_{\phi_0}^{\phi_d+m\pi} \frac{\sqrt{f(\phi)}}{g(\phi)\sqrt{G(\phi)}}\,\mathrm{d}\phi. \tag{4.13}$$

For Case I considered here, $l \leq G'(\phi) = 2h(\phi)/g(\phi) \leq L$ for some $L > l > 0$, and hence, $G(\phi) \geq l(\phi - \phi_0)$ for $\phi \geq \phi_0$. Therefore, both improper integrals in $H_m(0)$ converge.

(ii) It is clear that $H_m(0)$ is increasing in m. It follows from $0 \leq G(\phi) \leq L(\phi - \phi_0)$ for $\phi \geq \phi_0$ that the two integrals in $H_m(0)$ diverge as $m \to \infty$. □

Our main result below follows from Proposition 4.8 and Lemma 4.9.

Theorem 4.10. *Assume $\gamma_1 > |\gamma_2|$. For any given $m \geq 0$, one has*

(i) if $H_m(0) < (v_d - v_0)d$, then BVP (2.12) and (2.13) has no monotone m-winding solution.

(ii) if $H_m(0) \geq (v_d - v_0)d$, then BVP (2.12) and (2.13) has a unique monotone m-winding solution. In particular, if $m \geq m_0$ for some m_0, then BVP (2.12) and (2.13) has a unique monotone m-winding solution.

Remark 4.3. Note that, the second statement in (ii) provides co-existence of infinite many monotone winding solutions for any given $v_d - v_0$. It would be interesting to understand the stability of these solutions. □

Remark 4.4. Note that larger K_j's and/or smaller $|\alpha_j|$'s make $H_m(0)$ in (4.13) larger, and hence, the condition $H_m(0) \geq (v_d - v_0)d$ is easier to meet. Physically this makes sense. In fact, for large K_j's and/or smaller $|\alpha_j|$'s, the nematic material is elastically stronger (or more closer to solid). Therefore, the material has a large force to stay aligned or form *monotone* windings once it is forced by a shear speed $v_d - v_0$. Likewise, for small K_j's and/or large $|\alpha_j|$, the nematic material is close to liquid, and hence, is harder to stay monotonically. □

4.2.2 Non-monotone m-winding solutions for fixed $m \geq 0$

We now consider the existence of non-monotone m-winding solutions when $H_m(0) < (v_d - v_0)d$ (see the arc c in Figure 6). For such a solution, $\phi(y)$ has a minimum, say, α. Following the procedure in the previous part, one now sets

$$L_m(\alpha) = N_m(\alpha) \cdot \hat{N}_m(\alpha), \tag{4.14}$$

where $N_m(\alpha)$ is defined in (4.6) and recast below

$$\begin{aligned} N_m(\alpha) &= 2N_1(\alpha) + N_2(\alpha; m) \\ &= 2\int_\alpha^{\phi_0} \frac{\sqrt{f(\phi)}}{\sqrt{G(\phi) - G(\alpha)}} \mathrm{d}\phi + \int_{\phi_0}^{\phi_d + m\pi} \frac{\sqrt{f(\phi)}}{\sqrt{G(\phi) - G(\alpha)}} \mathrm{d}\phi, \end{aligned}$$

and

$$\begin{aligned} \hat{N}_m(\alpha) &= 2\hat{N}_1(\alpha) + \hat{N}_2(\alpha; m) \\ &= 2\int_\alpha^{\phi_0} \frac{\sqrt{f(\phi)}}{g(\phi)\sqrt{G(\phi) - G(\alpha)}} \mathrm{d}\phi + \int_{\phi_0}^{\phi_d + m\pi} \frac{\sqrt{f(\phi)}}{g(\phi)\sqrt{G(\phi) - G(\alpha)}} \mathrm{d}\phi. \end{aligned}$$

It is easy to check that $L_m(\alpha)$ is well-defined for $\alpha < \phi_0$ and

$$\lim_{\alpha \to \phi_0^-} L_m(\alpha) = H_m(0). \tag{4.15}$$

Similar to Proposition 4.8, one has

Proposition 4.11. *BVP (2.12) and (2.13) has a non-monotone m-winding solution associated to the minimum α if and only if α is a solution of $L_m(\alpha) = (v_d - v_0)d$.*

The following result gives the existence of non-monotone m-winding solutions.

Theorem 4.12. *Assume $\gamma_1 > |\gamma_2|$ and fix $m \geq 0$. If $H_m(0) < (v_d - v_0)d$, then BVP (2.12) and (2.13) has at least one non-monotone m-winding solutions.*

Proof. It is shown in the proof of Theorem 4.5 that $\lim_{\alpha\to-\infty} N_1(\alpha) = +\infty$. Note that $\hat{N}_1(\alpha) \geq C_0 N_1(\alpha)$ for some constant since g is bounded from above. Thus $\lim_{\alpha\to-\infty} L_m(\alpha) = +\infty$. The statement then follows from (4.15). □

Remark 4.5. For small K_j's and/or large $|\alpha_j|$ (so that $H_m(0) < (v_d - v_0)d$ is easier to hold), the nematic material is closer to liquid. While it is harder for such a nematic material to form *monotone* winding alignment as commented in Remark 4.4, it is easier to form *non-monotone* winding. □

4.2.3 Existence and multiplicity of m-winding solutions

Combining Theorem 4.10 and Theorem 4.12, one has, for any $m \geq 0$, there exists *at least* one m-winding solutions under the condition $\gamma_1 > |\gamma_2|$. There always are infinitely many winding solutions (see Remark 4.3) with different m. We do not know if monotone and non-monotone m-winding solutions can *co-exist*. For any $m \geq 0$, while monotone m-winding solution is unique, there may be multiple non-monotone m-winding solutions; More precisely, we will show that the function $L_m(\alpha)$ may have infinity critical points, which means BVP (2.12) and (2.13) has multiple solutions for some values of $(v_d - v_0)$.

Set

$$\hat{l}(x) = \hat{l}_0 + \hat{l}_1 x^2 + \hat{l}_2 x^4 + \hat{l}_3 x^6, \tag{4.16}$$

where

$$\begin{aligned}
\hat{l}_0 &= \alpha_2(-\alpha_2 + \alpha_4 + \alpha_5)K_1 \\
&\quad + [\alpha_1(-2\alpha_2 + 2\alpha_3) + \alpha_2(-3\alpha_2 - 2\alpha_3 + \alpha_4 + \alpha_5) + \alpha_3(2\alpha_3 + 2\alpha_5)]K_3, \\
\hat{l}_1 &= [\alpha_1(-\alpha_2 + 2\alpha_3) + \alpha_2(2 - 4\alpha_2 - 4\alpha_3 + \alpha_4 + \alpha_6) + \alpha_3(2 + \alpha_4 + \alpha_5)]K_1 \\
&\quad + [\alpha_1(8\alpha_2 - 2\alpha_3) + \alpha_2(4\alpha_2 + 4\alpha_3 - \alpha_4 - 2\alpha_5 + 2\alpha_6) + \alpha_3(-\alpha_4 - 3\alpha_5 + \alpha_6)]K_3, \\
\hat{l}_2 &= [\alpha_1(4\alpha_2 - 2\alpha_3) + \alpha_2(\alpha_2 + 2\alpha_3 - \alpha_5 + \alpha_6) + \alpha_3(\alpha_3 - \alpha_5 + \alpha_6)]K_1 \\
&\quad + [\alpha_1(-8\alpha_2 - 2\alpha_3) + \alpha_2(7\alpha_2 - 2\alpha_3 + \alpha_5 - \alpha_6) + \alpha_3(-\alpha_3 + \alpha_5 - \alpha_6)]K_3, \\
\hat{l}_3 &= 2\alpha_1(\alpha_2 + \alpha_3)(K_3 - K_1).
\end{aligned}$$

Theorem 4.13. *Assume $\gamma_1 > |\gamma_2|$ and $\hat{l}(x) \geq 0$ for all $|x| \leq 1$ where $\hat{l}(x)$ is defined in (4.16). Then there are infinitely many $\alpha \leq \phi_0$ such that $L'(\alpha) = 0$.*

Proof. It follows from (4.14) that

$$L'_m(\alpha) = N'_m(\alpha)\hat{N}_m(\alpha) + N_m(\alpha)\hat{N}'_m(\alpha),$$

where $N_m(\alpha) > 0$ and $\hat{N}_m(\alpha) > 0$, so the monotonicity of the function $L_m(\alpha)$ is determined by functions $N'_m(\alpha)$ and $\hat{N}'_m(\alpha)$. From the proof of Theorem 4.7 and with the function $g(\phi) > 0$ bounded, there are infinitely many α, such that $N'_m(\alpha) = 0$.

The following we will discuss the monotonicity of the function $\hat{N}'_m(\alpha)$. By the same method, we still divide $\hat{N}_1(\alpha)$ into two terms,

$$\begin{aligned}\hat{N}_1(\alpha) =& \hat{N}_{11}(\alpha) + \hat{N}_{12}(\alpha) \\ =& \int_{\alpha}^{\frac{\pi}{2}} \frac{\sqrt{f(\phi)}}{g(\phi)\sqrt{G(\phi)-G(\alpha)}} \mathrm{d}\phi + \int_{\frac{\pi}{2}}^{\phi_0} \frac{\sqrt{f(\phi)}}{g(\phi)\sqrt{G(\phi)-G(\alpha)}} \mathrm{d}\phi.\end{aligned}$$

The derivative of the first term of $\hat{N}_1(\alpha)$ is

$$\hat{N}'_{11}(\alpha) = D(\alpha)\left[\frac{-\sqrt{f(\frac{\pi}{2})}}{g(\frac{\pi}{2})D(\frac{\pi}{2})\sqrt{G(\frac{\pi}{2})-G(\alpha)}} + \frac{1}{2}\int_{\alpha}^{\frac{\pi}{2}} \frac{B(\phi)\sin(2\phi)}{\sqrt{G(\phi)-G(\alpha)}}\, d\phi\right],$$

where

$$B(\phi) = \frac{f'(\phi)g(\phi)D(\phi) - 2f(\phi)[g'(\phi)D(\phi) + g(\phi)D'(\phi)]}{D^2(\phi)g^2(\phi)\sqrt{f(\phi)}} = \frac{\hat{l}(\cos^2\phi)}{D^2(\phi)g^3(\phi)\sqrt{f(\phi)}}.$$

And

$$\begin{aligned}\hat{l}(\cos^2\phi) =& (K_3 - K_1)(\gamma_1 + \gamma_2\cos 2\phi)g(\phi) \\ &- 2[K_3 + (K_1 - K_3)\cos^2\phi](\alpha_1\cos 2\phi - \gamma_2)(\gamma_1 + \gamma_2\cos 2\phi) \\ &+ 2[K_3 + (K_1 - K_3)\cos^2\phi][2\gamma_2 g(\phi) + \gamma_2\cos 2\phi(-\alpha_1 - \gamma_2 + 2\alpha_1\cos 2\phi)] \\ =& \hat{l}_0 + \hat{l}_1\cos^2\phi + \hat{l}_2\cos^4\phi + \hat{l}_3\cos^6\phi.\end{aligned}$$

From Lemma 4.6, we get

$$\hat{N}'_{11}(-\frac{m\pi}{2}) = \begin{cases} < 0, & m \textit{ is a sufficiently large even number}, \\ > 0, & m \textit{ is a sufficiently large odd number}. \end{cases} \tag{4.17}$$

As well, we easily get

$$\lim_{\alpha\to-\infty} \hat{N}'_1(\alpha) = 0, \quad \lim_{\alpha\to-\infty} \hat{N}'_2(\alpha; m) = 0.$$

Then $\hat{N}'_m(\alpha)$ changes sign infinitely many times as $\alpha \to -\infty$. By the classical Zero Theorem, there are infinitely many α, such that $L'_m(\alpha) = 0$. □

Remark 4.6. Similarly to Remark 4.2, we comment that the assumption that $\hat{l}(x) > 0$ for $|x| \leq 1$ is possible. For example, if $\alpha_3 \geq \alpha_2 > 0$, $\alpha_1 < 0$, $\alpha_4 \gg 0$, and $K_1 > K_3$, then $\hat{l}_0 > 0$, $\hat{l}_1 + \hat{l}_2 x^2 + \hat{l}_3 x^4 > 0$ for any x; in particular, $\hat{l}(x) > 0$ for any x.

Remark 4.7. The multiple solutions are responsible for hysteresis phenomena, as in [12].

5 Case II: $|\gamma_2| = \gamma_1$ for fixed $a > 0$ only

As mentioned before, for simplicity, we will consider BVP (2.16) and (2.17) with fixed $a > 0$ and treat $(v_d - v_0)$ as a design parameter determined from (2.15).

This case is similar to Case I with some differences. We will present the results and comment on the differences from those in Case I. We will only consider the case with $\gamma_2 < 0$ so $(n\pi, 0)$ is an equilibrium for any integer n and the phase plane portrait with representative solutions is sketched in Figure 7. Recall we have assumed that $(\phi_0, 0)$ and $(\phi_d, 0)$ are not equilibria.

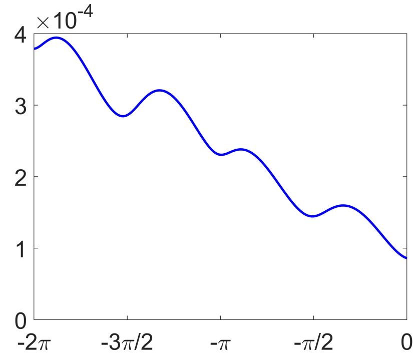

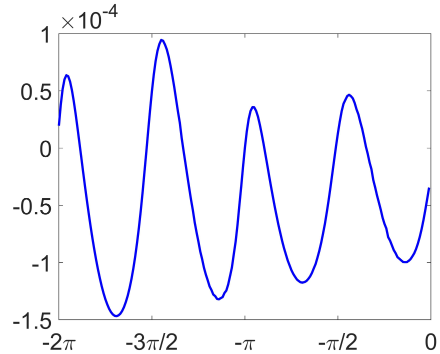

Figure 12: *An example of graphs of $L_m(\alpha)$ and $L'_m(\alpha)$: left for $L_m(\alpha)$ and right for $L'_m(\alpha)$.*

5.1 Monotone m-winding solutions for fixed $m \geq 0$

Similar to Section 4, one has that the set of monotone m-winding solutions starting at (ϕ_0, η_0) for some $\eta_0 \geq 0$ is a monotone m-winding solution if and only if $M_m(c) = \sqrt{a}d$ has a solution c where

$$M_m(c) = \int_{\phi_0}^{\phi_d + m\pi} \frac{\sqrt{f(\phi)}}{\sqrt{G(\phi) + c}} \mathrm{d}\phi. \tag{5.1}$$

as defined in (4.4) and $c \geq 0$ is related to η_0 in (4.2).

In the same way as Lemma 4.1, one has

Lemma 5.1. *For fixed $m \geq 0$, $M_m(c)$ is decreasing in $c \geq 0$, and*

$$\lim_{c \to +\infty} M_m(c) = 0 \quad \textit{and} \quad M_m(0) < \infty.$$

Similarly, one defines $a_m > 0$ as in (4.5)

$$\sqrt{a_m} = \frac{1}{d} \int_{\phi_0}^{\phi_d + m\pi} \frac{\sqrt{f(\phi)}}{\sqrt{G(\phi)}} \mathrm{d}\phi = \frac{M_m(0)}{d}. \tag{5.2}$$

The main result for this case is as follows.

Theorem 5.2. *Assume $\gamma_1 = |\gamma_2|$. For any given $m \geq 0$, one has*
(i) if $a > a_m$, then BVP (2.16) and (2.17) has no monotone m-winding solution;
(ii) if $a \leq a_m$, then BVP (2.16) and (2.17) has a unique monotone m-winding solution.

5.2 Non-monotone m-winding solutions for fixed $m \geq 0$

Concerning non-monotone solutions, there is a key difference between Case II and Case I.

Following Section 4 for Case I, but for $\alpha < \phi_0$ and $\alpha \neq n\pi$, let

$$N_m(\alpha) = 2N_1(\alpha) + N_2(\alpha; m) = 2\int_{\alpha}^{\phi_0} \frac{\sqrt{f(\phi)}}{\sqrt{G(\phi) - G(\alpha)}} \mathrm{d}\phi + \int_{\phi_0}^{\phi_d + m\pi} \frac{\sqrt{f(\phi)}}{\sqrt{G(\phi) - G(\alpha)}} \mathrm{d}\phi. \tag{5.3}$$

Note that, since $G'(n\pi) = 0$, $N_m(n\pi)$ diverges. One can establish the next result easily.

Lemma 5.3. *The function $N_m(\alpha)$ is well-defined for $\alpha \neq n\pi$,*

$$\lim_{\alpha\to\phi_0^-} N_m(\alpha) = M_m(0) \quad \textit{and} \quad \lim_{\alpha\to n\pi} N_m(\alpha) = +\infty.$$

Proof. The first limit can be established as in Lemma 4.3. Since $G'(n\pi) = 0$, one has

$$G(\phi) - G(n\pi) = O(\phi - n\pi)^2,$$

which implies the integral for $N_1(\alpha)$ diverges, and hence, the second limit holds. □

Between any two equilibria $((n-1)\pi, 0)$ and $(n\pi, 0)$ to the left of $(\phi_0, 0)$; that is, $n \leq 0$, let

$$a_{m,n} = \min\{N_m(\phi) : \phi \in ((n-1)\pi, n\pi)\}.$$

It follows from Lemma 5.3 that $a_{m,n}$ exists for any n and, in particular, for $n \leq 0$.

The next result is on non-monotone m-winding solutions.

Theorem 5.4. *Assume $\gamma_1 = |\gamma_2|$. If $a > a_m$, then BVP (2.16) and (2.17) has at least one non-monotone m-winding solution associated to some $\alpha \in (0, \phi_0)$. Moreover, for any $n \leq 0$,*

(i) if $a < a_{m,n}$, then there is no non-monotone m-winding solution associated to some $\alpha \in ((n-1)\pi, n\pi)$;

(ii) if $a = a_{m,n}$, then there is one non-monotone m-winding solution associated to the minimum point of $N_m(\alpha)$ for $\alpha \in ((n-1)\pi, n\pi)$;

(iii) if $a > a_{m,n}$, then there are at least two non-monotone m-winding solution associated to some $\alpha \in ((n-1)\pi, n\pi)$.

Proof. If $a > a_m$, then $N_m(\alpha) < \sqrt{a}d$ for α close to ϕ_0. Lemma 5.3 then implies the first statement. Others follow from the definition of $a_{m,n}$ and Intermediate Value Theorem. □

Note that the underlying mechanism of the result for a near $a_{m,n}$ is the saddle-node bifurcation. A study of stability of these multiple solutions in the time evolution system is an interesting and important task.

Remark 5.1. (a) Statement (iii) of the theorem implies that, as $a \to \infty$ (there would be infinite many pairs of (m, n) with $a > a_{m,n}$), the number of solutions goes to infinity too.

(b) Here is an interesting observation: While Theorem 4.7 for the existence of multiple solutions of BVP (2.16) and (2.17) was not easy to obtained, the possibility of existence of multiple non-monotone m-winding solutions for Case I follows easily from continuity (by perturbing $\gamma_1 = |\gamma_2|$ to $\gamma_1 > |\gamma_2|$) and part (a) above.

6 Case III: $|\gamma_2| > \gamma_1$ with fixed $a > 0$ only

Similarly to Section 5, for simplicity, we will consider BVP (2.16) and (2.17) with fixed $a > 0$, so one can make $(v_d - v_0)$ as a design parameter determined from (2.15).

Recall from Proposition 3.3 that, in this case, system (3.2) has equilibria $(\phi^* + n\pi, 0)$ and $(-\phi^* + n\pi, 0)$ for all integers n, where $\phi^* = \frac{1}{2}\arccos(-\gamma_1/\gamma_2) \in (0, \pi/2)$. Furthermore, if $\gamma_2 > 0$, then $(\phi^* + n\pi, 0)$ are centers and $(-\phi^* + n\pi, 0)$ are saddles; if $\gamma_2 < 0$, then $(\phi^* + n\pi, 0)$ are saddles and $(-\phi^* + n\pi, 0)$ are centers.

6.1 Subcase III1. $G(\pi) = G(0)$: Heteroclinic cycles

In this case, the adjacent saddles are connected by heteroclinic cycles that enclose periodic orbits around the centers. In particular, the heteroclinic cycles separate the phase plane into three major regions: the one above all heteroclinic cycles R_+, the one enclosed by heteroclinic cycles R_0, and the one below all heteroclinic cycles R_-. See Figure 8 for some illustrations.

Monotone m-winding solutions. Recall we consider only $m \geq 0$.

Proceeding as in Section 4.1.1, one has that the set of monotone m-winding solutions is in one-to-one correspondence with the set of solutions c of $M_m(c) = \sqrt{a}d$ where

$$M_m(c) = \int_{\phi_0}^{\phi_d + m\pi} \frac{\sqrt{f(\phi)}}{\sqrt{G(\phi) + c}} \mathrm{d}\phi, \tag{6.1}$$

is defined exactly as that in (4.4) but the range for c is different; more precisely,

(a) If there is no saddle $(\hat{\phi}, 0)$ with $\hat{\phi} \in [\phi_0, \phi_d + m\pi]$, then $c \in [\hat{c}, \infty)$ where

$$\hat{c} = \max\{-G(\phi_0), -G(\phi_d)\} = \max\{0, -G(\phi_d)\}. \tag{6.2}$$

So $\hat{c}$ corresponds to the larger level of the Hamiltonian function among $(\phi_0, 0)$ and $(\phi_d, 0)$.

(b) If there is a saddle $(\hat{\phi}, 0)$ with $\hat{\phi} \in [\phi_0, \phi_d + m\pi]$, then $c \in (c^*, \infty)$ where

$$c^* = -G(\hat{\phi}) > \hat{c}. \tag{6.3}$$

The reason for $c^* > \hat{c}$ is that the level of Hamiltonian function along the heteroclinic orbit is larger than those $(\phi_0, 0)$ and $(\phi_d, 0)$ in the case (a).

We comment that, $m = 0$ is necessary for case (a) since if $(\hat{\phi}, 0)$ is a saddle and $\hat{\phi} < \phi_0 < \phi_d < \hat{\phi} + \pi$, then $\phi_0 < \hat{\phi} + \pi < \phi_d + \pi$.

The next result follows from the definition of $M_m(c)$.

Lemma 6.1. *For fixed $m \geq 0$, $M_m(c)$ is decreasing in c and $\lim_{c \to +\infty} M_m(c) = 0$.*

Lemma 6.2. *Fix $m \geq 0$.*

(a) If there is no saddle $(\hat{\phi}, 0)$ with $\hat{\phi} \in [\phi_0, \phi_d]$, then $M_0(\hat{c})$ is finite, and hence,

$$\begin{aligned} \sqrt{\hat{a}} =& \frac{1}{d} \int_{\phi_0}^{\phi_d} \frac{\sqrt{f(\phi)}}{\sqrt{G(\phi) + \hat{c}}} \mathrm{d}\phi = \frac{M_0(\hat{c})}{d}, \\ \sqrt{a^*} =& \frac{1}{d} \int_{\phi_0}^{\phi_d} \frac{\sqrt{f(\phi)}}{\sqrt{G(\phi) + c^*}} \mathrm{d}\phi = \frac{M_0(c^*)}{d} \end{aligned} \tag{6.4}$$

are well defined and $a^* < \hat{a}$;

(b) If there is a saddle $(\hat{\phi}, 0)$ with $\hat{\phi} \in [\phi_0, \phi_d + m\pi]$, then

$$\lim_{c \to c^* = -G(\hat{\phi})} M_m(c) = \infty.$$

Proof. (a) The statement that $M_m(\hat{c})$ follows from the same argument as for Lemma 4.1 since ϕ_0 and ϕ_d are not critical points of G. Since $c^* > \hat{c}$, one has $a^* < \hat{a}$.

(b) For the statement, one then has, near $\hat{\phi}$,

$$G(\phi) + c \to G(\phi) - G(\hat{\phi}) = O(\phi - \hat{\phi})^2,$$

and hence, the integral in the definition of $M_m(c)$ diverges as $c \to c^*$. □

One obtains the next result directly.

Theorem 6.3. *Let $|\gamma_2| > \gamma_1$ and fix $m \geq 0$.*

(a) Assume there is no saddle $(\hat{\phi}, 0)$ with $\hat{\phi} \in [\phi_0, \phi_d]$. One has

(i) if $a > \hat{a}$, then BVP (2.16) and (2.17) has no monotone 0-winding solution;

(ii) if $a \leq \hat{a}$, then BVP (2.16) and (2.17) has a unique monotone 0-winding solution; Moreover, if $a^* \leq a \leq \hat{a}$, then the orbit lies in R_0; if $a < a^*$, then the orbit lies in R_+.

(b) Assume there is a saddle $(\hat{\phi}, 0)$ with $\hat{\phi} \in [\phi_0, \phi_d + m\pi]$. Then BVP (2.16) and (2.17) always has a unique monotone m-winding solution, and the orbit lies entirely in R_+.

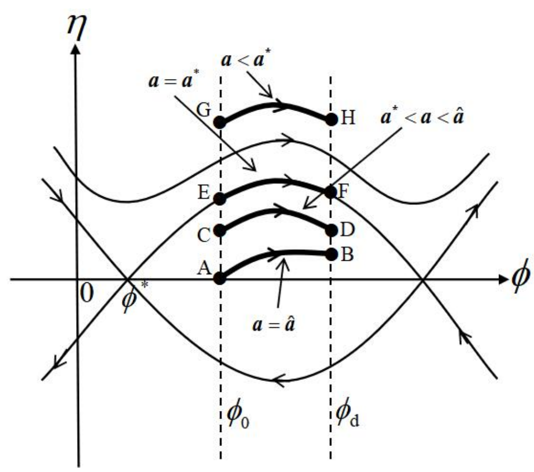

Figure 13: *Representative orbits from Theorem 6.3 for $\gamma_2 > 0$: arc AB associated to $a = \hat{a}$, arc CD associated to $a \in (a^*, \hat{a})$, arc EF associated to $a = a^*$, and arc GH associated to $a < a^*$.*

Non-monotone or vibrating solutions. This only occurs for the case (a) when there is no saddle $(\hat{\phi}, 0)$ with $\hat{\phi} \in [\phi_0, \phi_d]$, and hence, such solutions are 0-winding. So we will classify the solutions as *vibrating solutions*. For simplicity, we will consider the case where

$$\gamma_2 > \gamma_1 > 0,\ \phi^* < \phi_0 < \phi_d < \phi^* + \pi,\ G(\phi_d) < 0 = G(\phi_0). \tag{6.5}$$

Note that $\gamma_2 > \gamma_1 > 0$ implies that $(\phi^* + n\pi, 0)$ are saddles, and $G(\phi_d) < 0 = G(\phi_0)$ implies that $\hat{c} = 0$ where $\hat{c}$ is defined in (6.2).

Lemma 6.4. *Assume (6.5). Then, for any $\alpha \in (\phi^*, \phi_0)$, there exists $\beta = \beta(\alpha) \in (\phi_0, \phi^* + \pi)$ such that $G(\alpha) = G(\beta)$.*

Similar to the treatment in Sections 4 and 5 for non-monotone solutions, we introduce, for any $\alpha \in (\phi^*, \phi_0)$, let

$$V(\alpha) = V_l(\alpha) + V_0(\alpha) + V_l(\alpha),$$

where

$$\begin{aligned} V_l(\alpha) &= \int_{\alpha}^{\phi_0} \frac{\sqrt{f(\phi)}}{\sqrt{G(\phi) - G(\alpha)}} \mathrm{d}\phi, \\ V_0(\alpha) &= \int_{\phi_0}^{\phi_d} \frac{\sqrt{f(\phi)}}{\sqrt{G(\phi) - G(\alpha)}} \mathrm{d}\phi, \\ V_r(\alpha) &= \int_{\phi_d}^{\beta(\alpha)} \frac{\sqrt{f(\phi)}}{\sqrt{G(\phi) - G(\alpha)}} \mathrm{d}\phi. \end{aligned} \tag{6.6}$$

Note that

$$\lim_{\alpha \to \phi_0} V_l(\alpha) = M_0(\hat{c}) = M_0(0).$$

Set $\hat{a}_0 = \hat{a}$ and, for $n \geq 1$, define $\hat{a}_n$ by

$$\begin{aligned} \sqrt{\hat{a}_{2k}}d =& 2kV(\phi_0) + V_0(\phi_0) = (2k+1)V(\phi_0) - V_r(\phi_0), \\ \sqrt{\hat{a}_{2k+1}}d =& (2k+1)V(\phi_0) + V_r(\phi_0). \end{aligned} \tag{6.7}$$

For example,

$$\begin{aligned} \sqrt{\hat{a}_1}d =& V(\phi_0) + V_r(\phi_0), \\ \sqrt{\hat{a}_2}d =& 2V(\phi_0) + V_0(\phi_0) = 3V(\phi_0) - V_r(\phi_0). \end{aligned}$$

Lemma 6.5. *One has $\{\hat{a}_n\}$ is strictly increasing in n.*

Theorem 6.6. *Under the assumption in (6.5), one has, for $k \geq 0$,*

(i) if $a \geq \hat{a}_{2k}$, then there exists at least one (r,l)-$2k$-vibrating solution;
if $a > \hat{a}_{2k}$, then there exists at least one (l,l)-$(2k+1)$-vibrating solution;

(ii) if $a \geq \hat{a}_{2k+1}$, then there exists at least one (r,r)-$(2k+1)$-vibrating solution;
if $a > \hat{a}_{2k+1}$, then there exists at least one (l,r)-$(2k+2)$-vibrating solution.

Proof. We will illustrate the proof for case (i) with $k = 1$; that is, to show, if $a \geq \hat{a}_2$, then there exists (r,l)-2-vibrating solution and if $a > \hat{a}_2$, then there exists (l,l)-3-vibrating solution;

Recall, from (6.7), that

$$\sqrt{\hat{a}_2}d = 2V(\phi_0) + V_0(\phi_0) = 3V(\phi_0) - V_r(\phi_0).$$

Thus, for $a = \hat{a}_2$, $\phi = \phi_0$ is a solution of

$$2V(\alpha) + V_0(\alpha) = \sqrt{a}d.$$

Thus, the orbit (see ABCAB in Figure 14) from $(\phi_0, 0)$ tracing the full periodic orbit (ABCA in Figure 14) once and followed by the portion (AB in Figure 14) to $(\phi_d, 0)$ is the critical solution, which is an (r,l)-2-vibrating solution.

As the orbit ABCAB in Figure 14 for $a = \hat{a}_2$ expands to, say the orbit EFGDEFG in Figure 14 through $(\alpha, 0)$ for some $\alpha < \phi_0$, and then continue to close to the heteroclinic loop, the value of corresponding function $2V(\phi) + V_0(\phi)$ would approach ∞. Therefore, for $a > \hat{a}_2$, there is an α so that $2V(\alpha) + V_0(\alpha) = \sqrt{a}d$. The corresponding portion EFGDEFG in Figure 14 on the orbit $(\alpha, 0)$ is an (r, l)-2-vibrating solution.

Similarly, as the orbit ABCAB in Figure 14 for $a = \hat{a}_2$ expands to, say the orbit DEFGDEF in Figure 14 through $(\alpha, 0)$ for some $\alpha < \phi_0$, and then continue to close to the heteroclinic loop, the value of corresponding function $3V(\phi) - V_r(\phi)$ would approach ∞. Therefore, for $a > \hat{a}_2$, there is an α so that $3V(\alpha) - V_r(\alpha) = \sqrt{a}d$. The corresponding portion DEFGDEF in Figure 14 on the orbit $(\alpha, 0)$ is an (l, l)-3-vibrating solution. □

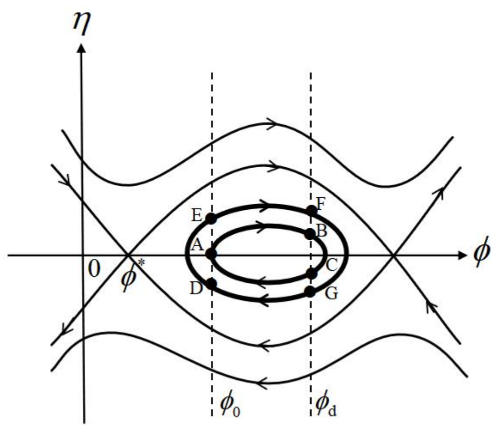

Figure 14: *Representative orbits from Theorem 6.6: arc ABC represents the r-1-vibrating solution associated to $a = \hat{a}_1$, arc EFG represents an r-1-vibrating solution for $a > \hat{a}_1$, arc DEFG represents a (l, r)-2-vibrating solution associated to $a > \hat{a}_1$; arc ABCAC represents the (r, l)-2-vibrating solution for $a = \hat{a}_2$, arc EFGDEFG represents an (r, l)-2-vibrating solution for $a > \hat{a}_2$, arc DEFGDEF represents a (l, l)-3-vibrating solution for $a > \hat{a}_2$.*

6.2 Subcase III2. $G(\pi) - G(0) \neq 0$: Homoclinic loops

We will consider only the case where $G(\pi) < G(0)$. For the other case, one can essentially reverse the phase plane portrait to exam in the similar way. Recall that $G(\pi) < G(0)$ implies that homoclinic loops lie on the right of the associated saddles. Thus, if ϕ-component of a solution $(\phi(y), \eta(y))$ has an interior minimum, then the orbit must lie inside a homoclinic loop; in particular, $(\phi_0, 0)$ must lie inside the homoclinic loop.

The treatments and the results on monotone solutions and vibrating solutions are similar to those in Subcase III1 with $G(\pi) = G(0)$. Therefore, we will only consider *non-monotone m-winding solutions* which lie outside any homoclinic loop.

Non-monotone m-winding solutions. Those are non-monotone solutions that do not lie inside a homoclinic loop. We also assume $\gamma_2 > 0$ so that $(\phi^* + n\pi, 0)$'s are saddles. The other cases can be handled in the similar way.

For any non-monotone solution $(\phi(y), \eta(y))$, $\phi(y)$ has a unique maximum $\phi = \beta$. For $\beta >$

$\phi_d + m\pi$, let

$$P_m(\beta) = P_1(\alpha; m) + 2P_2(\beta) = \int_{\phi_0}^{\phi_d+m\pi} \frac{\sqrt{f(\phi)}\mathrm{d}\phi}{\sqrt{G(\phi)-G(\beta)}} + 2\int_{\phi_d+m\pi}^{\beta} \frac{\sqrt{f(\phi)}\mathrm{d}\phi}{\sqrt{G(\phi)-G(\beta)}}. \tag{6.8}$$

One can then verify that, if $P_m(\beta) = \sqrt{a}d$, then $(\phi(y), \eta(y))$ is a non-monotone m-winding solution of BVP (2.16) and (2.17).

Denote R_n the region bounded by the curve $W^s(\phi^* + n\pi, 0) \cup W^u(\phi^* + n\pi, 0)$ and the curve $W^s(\phi^* + (n+1)\pi, 0) \cup W^u(\phi^* + (n+1)\pi, 0)$.

Theorem 6.7. *Assume $\gamma_2 > \gamma_1 > 0$ and $G(\pi) < G(0)$. Suppose $(\phi_d + m\pi, 0)$ lies between the two adjacent saddles $(\phi^* + n_m\pi, 0)$ and $(\phi^* + (n_m+1)\pi, 0)$. For any $n > n_m$, there is a_n^* such that,*

(i) if $a < a_n^*$, then there is no non-monotone solution that lies in R_n;

(ii) if $a = a_n^*$, then there is exactly one non-monotone solution that lies in R_n;

(iii) if $a > a_n^*$, then there are two non-monotone solutions that lie in R_n.

Furthermore, if $(\phi_0, 0)$ lies also between the two adjacent saddles (necessarily $m = n_m = 0$), then (for $n = n_m = 0$) there exist a_0^* and b_0^* with $a_0^* \leq b_0^* < \infty$ such that,

(i0) if $a < a_0^*$, then there is no non-monotone solution that lies in R_0;

(ii0) if $a = a_0^*$, then there is exactly one non-monotone solution that lies in R_0;

(iii0) if $a_0^* < a \leq b_0^*$, then there are two non-monotone solutions that lie in R_0;

(iv0) if $a \geq b_0^*$, then there is one non-monotone solution that lies in R_0.

Proof. As seen before, for any

$$\lim_{\beta \to \phi^* + n\pi} P_m(\beta) \to \infty.$$

For any $n > n_m$, let a_n^* be defined as

$$\sqrt{a_n^*}d = \min\Big\{P_m(\beta) : \beta \in (\phi^* + n\pi, \phi^* + (n+1)\pi)\Big\}.$$

Then, one has the statements (i), (ii), (iii).

If $(\phi_0, 0)$ and $(\phi_d, 0)$ lie between two same adjacent saddles, then $\phi^* < \phi_0 < \phi_d < \phi^* + \pi$. For $\beta \in (\phi_d, \phi^* + \pi)$ $P(\beta) \to \infty$ as $\beta \to \phi^* + \pi$ but $P_0(\beta) \to P_0(\phi_d) < \infty$ as $\beta \to \phi_0$. Let a_0^* and b_0^* be defined as

$$\sqrt{a_0^*}d = \min\Big\{P_m(\beta) : \beta \in (\phi^* + n\pi, \phi^* + (n+1)\pi)\Big\} \text{ and } \sqrt{b_0^*}d = P_0(\phi_d).$$

Then one has the claims (i0), (ii0), and (iii0). □

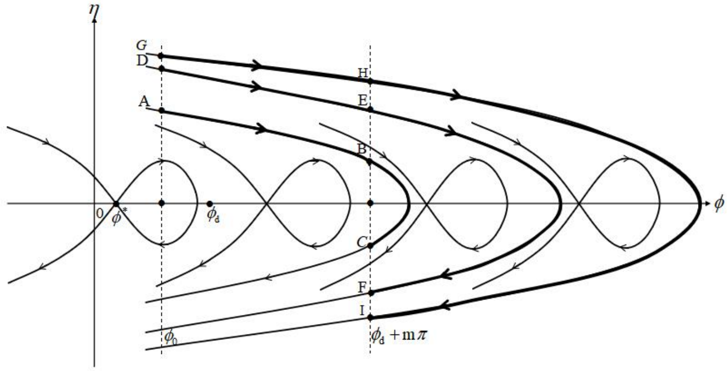

Figure 15: *Representative orbits of non-monotone m-winding solutions from Theorem 6.7: arcs ABC, DEF, GHI in different regions separated by homoclinic orbits.*

7 Conclusion

In this paper, we investigate the shear flow phenomena in nematic liquid crystals by the mathematical analysis of qualitative properties. A number of interesting properties are resulted from analysis of this governing equation. The success of our case study relies heavily on the theory of dynamical systems and, most importantly, some special structures of the Ericksen-Leslie equations for stationary shear flow. The Hamiltonian formulation of the system for ϕ – the angle of the director is a key contribution that allows us to approach the problem in a systematic way; in particular, we obtain a rather complete picture about how different types of solutions relate to physical parameters/quantities and how multiple solutions are created in a number of situations.

As far as detailed dynamic properties of nematic liquid crystals are concerned, it is still significant challenging to study. For shear flow considered in the simple setting of this paper, there are many unknowns revealed in this work. Of importance is an understanding of stability of these stationary solutions in time-evolution particularly when multiple solutions co-exist. Another direction is to investigate the influence of applied electric or magnetic forces on these stationary solutions, such as, in the application of LCD. It is our hope to continue this work and, among others, answer some of the concerns mentioned above.

Acknowledgments. J. Jiao and K. Huang thank the University of Kansas for its hospitality during their visits (J. Jiao from Sept. 2017-Oct. 2018 and K. Huang from Feb. 2018-Feb. 2019). J. Jiao is partially supported by a visiting scholarship from the China Scholarship Council and K. Huang is partially supported by the Joint Ph.D. Training Program sponsored by the China Scholarship Council. W. Liu's research is partially supported by Simons Foundation Mathematics and Physical Sciences-Collaboration Grants for Mathematicians #581822.

References

[1] A. Anzelius, Über die Bewegung der anisotropen Flüssigkeiten. *Uppsala Univ. Arsskr., Mat. och Naturvet.*, **1** (1931), pp. 1-84.

[2] R. J. Atkin, Poiseuille flow of liquid crystals of the nematic type. *Arch. Ration. Mech. Anal.* **38** (1970), pp. 224-240.

[3] R. Becker, X. Feng, A. Prohl, Finite element approximations of the Ericksen-Leslie model for nematic liquid crystal flow. *SIAM J. Numer. Anal.*, **46** (4) (2008), pp. 1704-1731.

[4] M. C. Calderer and C. Liu, Liquid crystal flow: dynamic and static configurations. *SIAM J. Appl. Math.*, **60** (2000), pp. 1925-1949.

[5] J. Q. Carou, B. R. Duffy, N. Mottram, S. K. Wilson, Steady flow of a nematic liquid crystal in a slowly varying channel, *Mol. Cryst. Liq. Cryst*, **438** (2005), pp. 1801-1813.

[6] S. Chandrasekhar, *Liquid Crystals*, 2nd ed., Cambridge University Press, 1992.

[7] G. Chen, T. Huang, and W. Liu, Poiseuille flow of nematic liquid crystals via the full Ericksen-Leslie model. *Arch. Ration. Mech. Anal.* **236** (2020), pp. 839-891.

[8] C. H. A. Cheng, L. H. Kellogg, S. Shkoller, and D. L. Turcotte, A liquid-crystal model for friction. *Proc. Natl. Acad. Sci.*, **105** (23) (2008), pp. 7930-7935.

[9] A. Ciferri, ed. *Liquid Crystallinity in Polymers: Principles and Fundamental Properties.* New York: VCH. 1991, pp. 438.

[10] P. A. Cruza, M. F. Tomé, I. W. Stewartb, S. McKeeb, A numerical method for solving the dynamic three-dimensional Ericksen-Leslie equations for nematic liquid crystals subject to a strong magnetic field. *J. Non-Newtonian Fluid Mech.*, **165** (2010), pp. 143-157.

[11] P. K. Currie, G. P. MacSithigh, The stability and dissipation of solutions for shearing flow of nematic liquid crystals. *Quart. J. Mech. Appl. Math.*, **32** (1979), pp. 499-511.

[12] T. Dorn and W. Liu, Steady-states for shear flows of a liquid-crystal model: Multiplicity, stability, and hysteresis. *J. Differential Equations*, **253** (2012), pp. 3184-3210.

[13] J. L. Ericksen, Transversely isotropic fluids. *Kolloid-Zeistschrift*, **173** (1960), pp. 117-122.

[14] J. L. Ericksen, Conservation laws for liquid crystals. *Trans. Soc. Rhel.*, **5** (1961), pp. 23-34.

[15] J. L. Ericksen, Equilibrium theory of liquid crystals. *Advances in Liquid Crystals*, **2** (1976), pp. 233-298.

[16] F. C. Frank, On the theory of liquid crystals. *Discuss. Faraday Soc.*, **25** (1958), pp. 19-28.

[17] G. Friedel, Les états mésomorphes de la matière. *Ann. Phys. (Paris)* **18** (1922), pp. 273-474.

[18] J. Fisher, A. G. Fredrickson, Interfacial effects on the viscosity of a nematic mesophase. *Mol. Cryst. Liq. Cryst.*, **8** (1969), pp. 267-284.

[19] P. G. de Gennes, Prost J. *The Physics of Liquid Crystals.* London: Oxford Univ. Press. 2nd ed., 1993, pp. 597.

[20] V. Girault, F. Guillen-Gonzalez, Mixed formulation, approximation and decoupling algorithm for a penalized nematic liquid crystals model. *Math. Comput.*, **80** (2011), pp. 781-819.

[21] O. Lehmann, Über fliessende Krystalle. *Zeitschrift für Physikalische Chemie*, **4** (1989), pp. 462-472.

[22] F. M. Leslie, Some constitutive equations for anisotropic fluids. *Quart. J. Mech. Appl. Math.*, **19** (1966), pp. 357-370.

[23] F. M. Leslie, Some constitutive equations for liquid crystals. *Arch. Rat. Mech. Anal.*, **28** (1968), pp. 265-283.

[24] F. M. Leslie, An analysis of a flow instability in nematic liquid crystals. *J. Phs. D: Appl.Phys.*, **9** (1976), pp. 925-937.

[25] F. M. Leslie, Theory of flow phenomena in liquid crystals. *Advances in Liquid Crystals*, **4** (1979), pp. 1-81.

[26] F. Lin and C. Wang, Recent developments of analysis for hydrodynamic flow of nematic liquid crystals. *Proc. R. Soc. Lond. A* , **372** (2014), pp. 20130361.

[27] F. Lin and C. Liu, Static and dynamic theories of liquid crystals. *J. Partial Differential Equations* **14** (2001), pp. 289-330.

[28] C. Liu and N. J. Walkington, Mixed methods for the approximation of liquid crystal flows. *ESAIM: Math. Model. Numer. Anal.*, **36** (2) (2002), pp. 205-222.

[29] C. W. Oseen, The theory of liquid crystals. *Trans. Faraday Soc.*, **29** (1933), pp. 883-899.

[30] T. W. Pan, Analysis of shear flow instability in nematic liquid crystals. *Ph. D. thesis*, University of Minnesota, (1990).

[31] T. W. Pan, On the existence of infinitely many limit points on the solution branch of planar shear flow of nematic. *J. Math. Anal. Appl.*, **208** (1997), pp. 120-140.

[32] T. W. Pan, Existence and multiplicity of radial solutions describing the equilibrium of nematic liquid crystals on annular domains. *J. Math. Anal. Appl.*, **245** (2000), pp. 266-281.

[33] F. Reinitzer, Beiträge zur Kenntnis des Cholesterins. *Monatsh. Chem.*, **9** (1988), pp. 421-441.

[34] F. Reinitzer, Contributions to the knowledge of cholesterol. Translation of Reference. *Liquid Crystal*, **5** (1989), pp. 7-18.

[35] I. W. Stewart, *The static and dynamic continuum theory of liquid crystals*, Taylor Francis, London, 2004.

[36] D. Vorländer, Einfluβ der molekularen Gestalt auf den krystallinisch-flüssigen Zustand. *Ber. Deutsch. Chem. Ges.*, **40** (1907), pp. 1970-1972.

[37] H. Zocher, Über die Einwirkung magnetischer, elektrischer und mechanischer Kräfte auf Mesophasen. *Physik. Zietschr.*, **28** (1927), pp. 790-796.